Supporting Information

Mechanistic investigation of nitridation-promoted reactivity and selectivity for propylene epoxidation in TS-1 catalysts: A theoretical study

Qiaoyun Qin,[a,b] Kai An,[a] Hongxia Liu,[c] Xueqiang Qi[a,*] and Baohe Wang[b,*]

[a] *College of Chemistry and Chemical Engineering, Chongqing University of Technology, Chongqing, 400054, China*

[b] *Collaborative Innovation Center of Chemical Science and Engineering, Tianjin University, Tianjin 300072, China; Key Laboratory for Green Chemical Technology of Ministry of Education, R&D Center for Petrochemical Technology, Tianjin University, Tianjin 300072, China*

[c] *School of Chemistry and Chemical Engineering, Wuhan Textile University, Wuhan, 430200, China*

* Corresponding author at: No. 69 Hongguang road, Banan district, Chongqing, China 400054
** Corresponding author at: No. 90 Weijin Road, Nankai District, Tianjin, China 300072
E-mail address: xqqi@cqut.edu.cn (Xueqiang Qi), wangbh@tju.edu.cn (Baohe Wang)

S1 Computational models

Structures of nitrided TS-1 model with tetrahedral Ti, Ti/defect and bipodal Ti sites

For TS-1 framework, there exist 12 crystallographic distinct tetrahedral sites (T-sites, and denoted as T1-T12), which are located on the ten membered ring straight pore channel (5.4×5.6 Å) and zigzag pore channel (5.1×5.5 Å), and regard as the active center for TS-1 catalyzed the epoxidation of propylene.[1] In order to take into account the confinement effect on the adsorption and reaction inside pores, a cluster of 86T containing the ten membered ring straight pore channel and zigzag pore channel is used to model the Ti-sites in TS-1. T10 crystallographic position was selected as the Ti site, which has been found to be the most energetically favored substitutional Ti location sites.[2-9] In the process of calculation, the center 16T of the 86T cluster is selected as the high level (atoms represented by balls) and treating with the high-level DFT method, while the rest of the extended framework is allocated to the low level (atoms shown in lines) and calculated using the universal force field (UFF) method. Meanwhile, the rest of the framework atoms processed by the low-level is frozen in their original lattice positions, while the atoms belonging to the central high-level is completely relaxed, as our previous calculation method.[10]

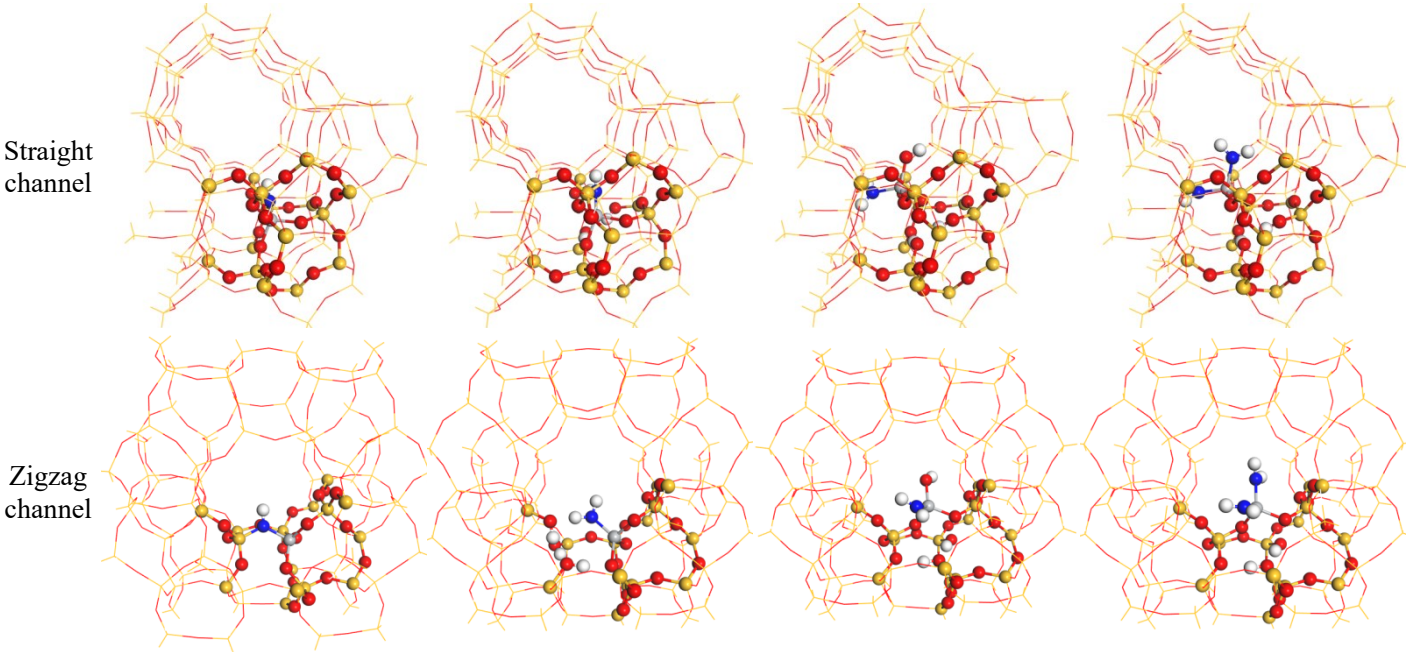

Fig. S1 Structures of nitrided TS-1 model with (a) tetrahedral Ti, (b) Ti/defect, (c) bipodal Ti and (d) double embedded bipodal Ti sites; view along the straight channel and zigzag channel (N=blue, Ti = light gray, Si = yellow, O = red and H = white).

TS-1 model with tetrahedral Ti, Ti/defect and bipodal Ti sites

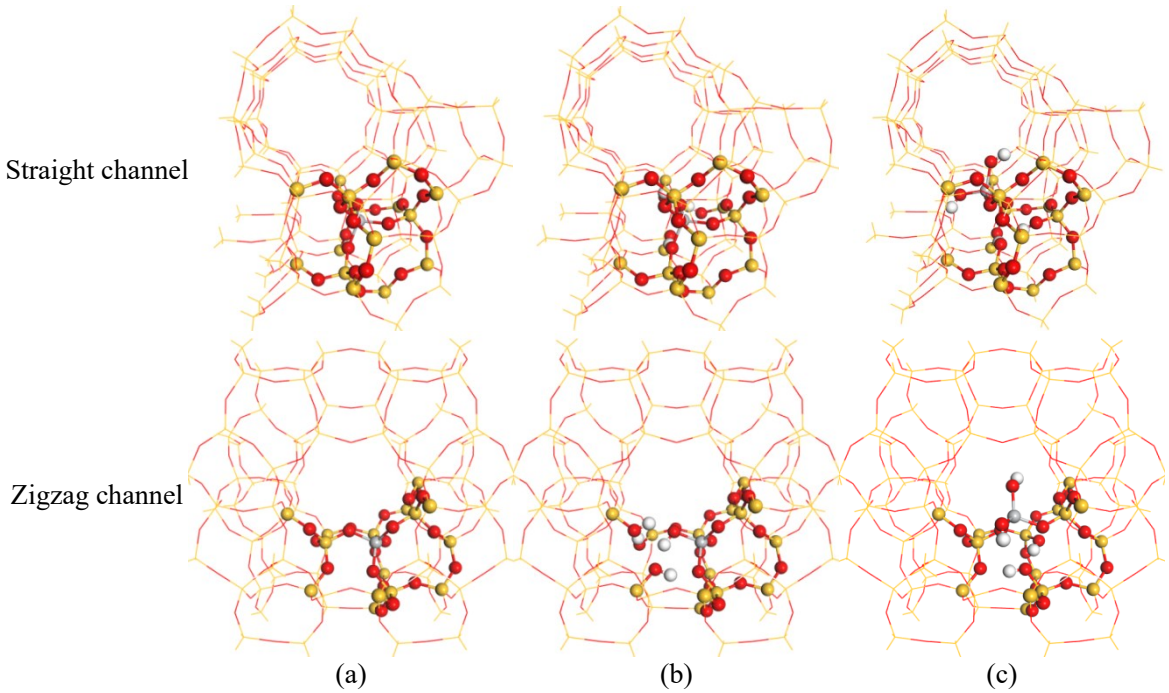

Fig. S2 The structures of TS-1 model with (a) tetrahedral Ti, (b) Ti/defect and (c) bipodal Ti sites. View along the straight channel and zigzag channel (Ti = light gray, Si = green, O = red, and H = white).

S2 Adsorption of possible species in propylene epoxidation

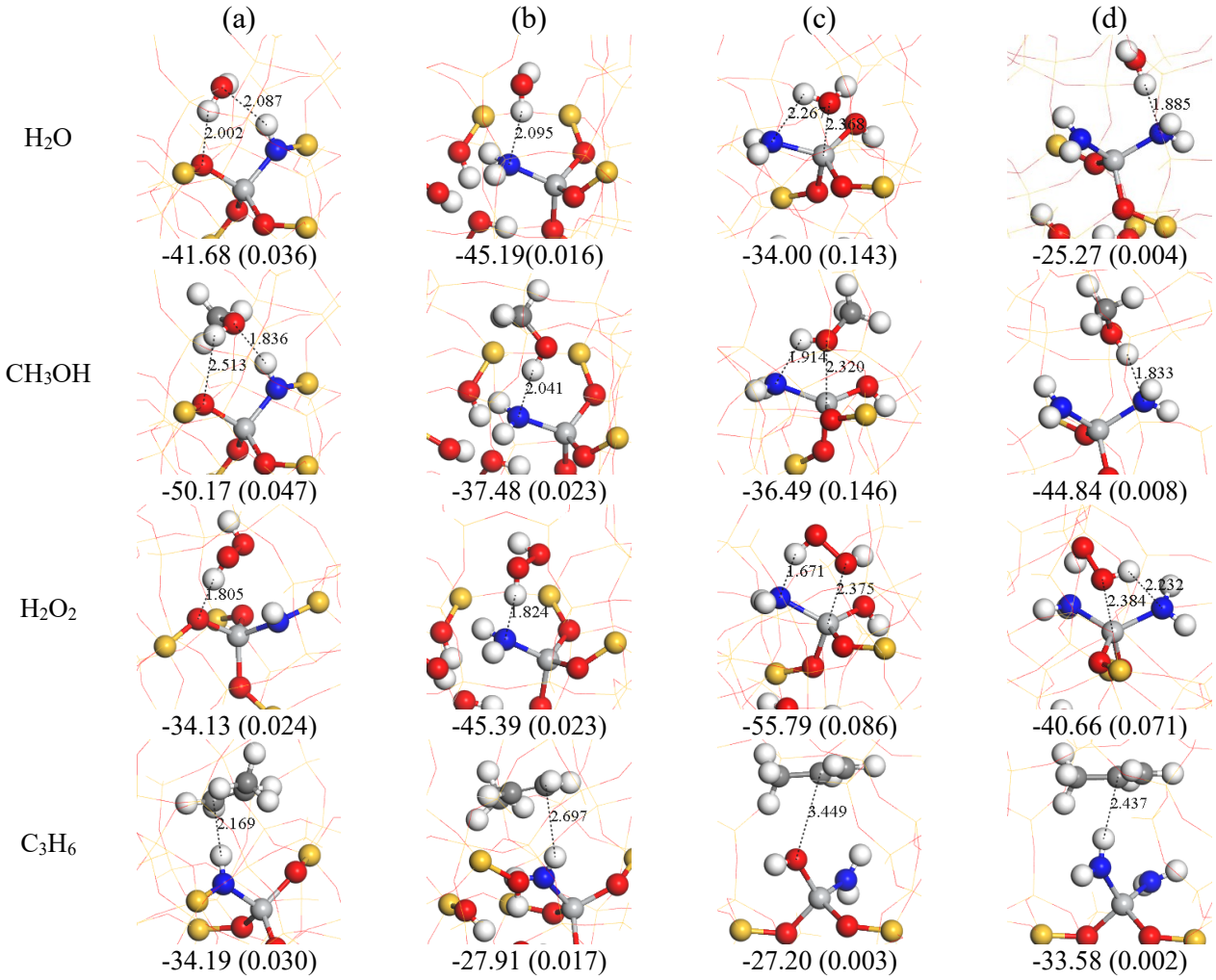

Fig. S3 The most stable adsorption configurations of H_2O, CH_3OH, H_2O_2 and C_3H_6 PO at the nitrided (a) tetrahedral Ti, (b) Ti/defect, (c) bipodal Ti and (d) double embedded bipodal Ti sites together with the free adsorption energies at 313 K and the Mulliken charger in parenthesis. The energy unit is in kJ/mol, and bond length is in Å (N = blue, Ti = light grey, C = grey, O = red, Si = yellow and H = white).

Table S1 Mulliken charger (*e*), adsorption free energy (G_{ads}, kJ/mol) and key structural parameter of H_2O, CH_3OH, H_2O_2 and C_3H_6 adsorption at the nitrided tetrahedral Ti, Ti/defect and bipodal Ti sites as well as double embedded bipodal Ti site at 313 K and those in parenthesis at 0 K.

Active sites	Species	Mulliken charge	G_{ads} (kJ/mol)	Adsorption detail	
				Modes	Length (Å)
Tetrhedral Ti site	H_2O	0.036	-41.68(-30.08)	H…O/O…H	2.002/2.087
	CH_3OH	0.047	-50.17(-29.20)	H…O/O…H	2.513/1.836
	H_2O_2	0.024	-34.13(-23.76)	H…O	1.805
	C_3H_6	0.030	-34.19(-11.04)	C…H	2.169

Ti/defect site	H_2O	0.016	-45.19(-35.95)	H…N	2.095
	CH_3OH	0.023	-37.48(-25.05)	H…N	2.041
	H_2O_2	0.024	-45.39(-33.91)	H…N	1.824
	C_3H_6	0.017	-27.91(-8.26)	C…H	2.697
Bipodal Ti site	H_2O	0.143	-34.00(-29.71)	O…Ti/H…N	2.368/2.267
	CH_3OH	0.146	-36.49(-28.73)	O…Ti/H…N	2.320/1.914
	H_2O_2	0.086	-55.79(-49.13)	O…Ti/H…N	2.375/1.671
	C_3H_6	0.003	-27.20(-5.98)	C…O	3.449
Double embedded bipodal Ti site	H_2O	0.004	-25.27(-18.13)	H…N	1.885
	CH_3OH	0.008	-44.84(-29.58)	H…N	1.833
	H_2O_2	0.071	-40.66(-34.43)	O…Ti/H…N	2.384/2.232
	C_3H_6	0.002	-33.58(-10.64)	C…H	2.437

Table S2 Mulliken charger (*e*), adsorption free energy (G_{ads}, kJ/mol) and key structural parameter of H_2O, CH_3OH, H_2O_2 and C_3H_6 at the tetrahedral Ti, Ti/defect and bipodal Ti sites at 313 K. These calculated results are obtained from our previous studies of non-nitrided modification.

Active sites	Species	Mulliken charge (*e*)	G_{ads} (kJ/mol)	Adsorption detail	
				Modes	Length (Å)
Tetrahedral Ti	H_2O	0.026	-24.96	H…O	2.208
	CH_3OH	0.027	-29.93	H…O	2.184
	H_2O_2	0.024	-26.50	H…O	1.864
	C_3H_6	0.020	-12.43	C…O	3.191
Ti/defect	H_2O	0.150	-49.08	H…O/O…Ti	2.376/2.362
	CH_3OH	0.026	-71.08	H…O	1.903
	H_2O_2	0.120	-48.18	H…O/O…Ti	1.764/2.356
	C_3H_6	0.023	-13.44	C…O	3.032
Bipodal Ti	H_2O	0.182	-43.30	O…Ti	2.245
	CH_3OH	0.169	-52.93	H…O/O…Ti	2.065/2.288
	H_2O_2	0.111	-55.65	H…O/O…Ti	1.708/2.356
	C_3H_6	0.007	-44.68	C…O	3.410

S3 Potential energy diagram for propylene epoxidation at the different Ti site

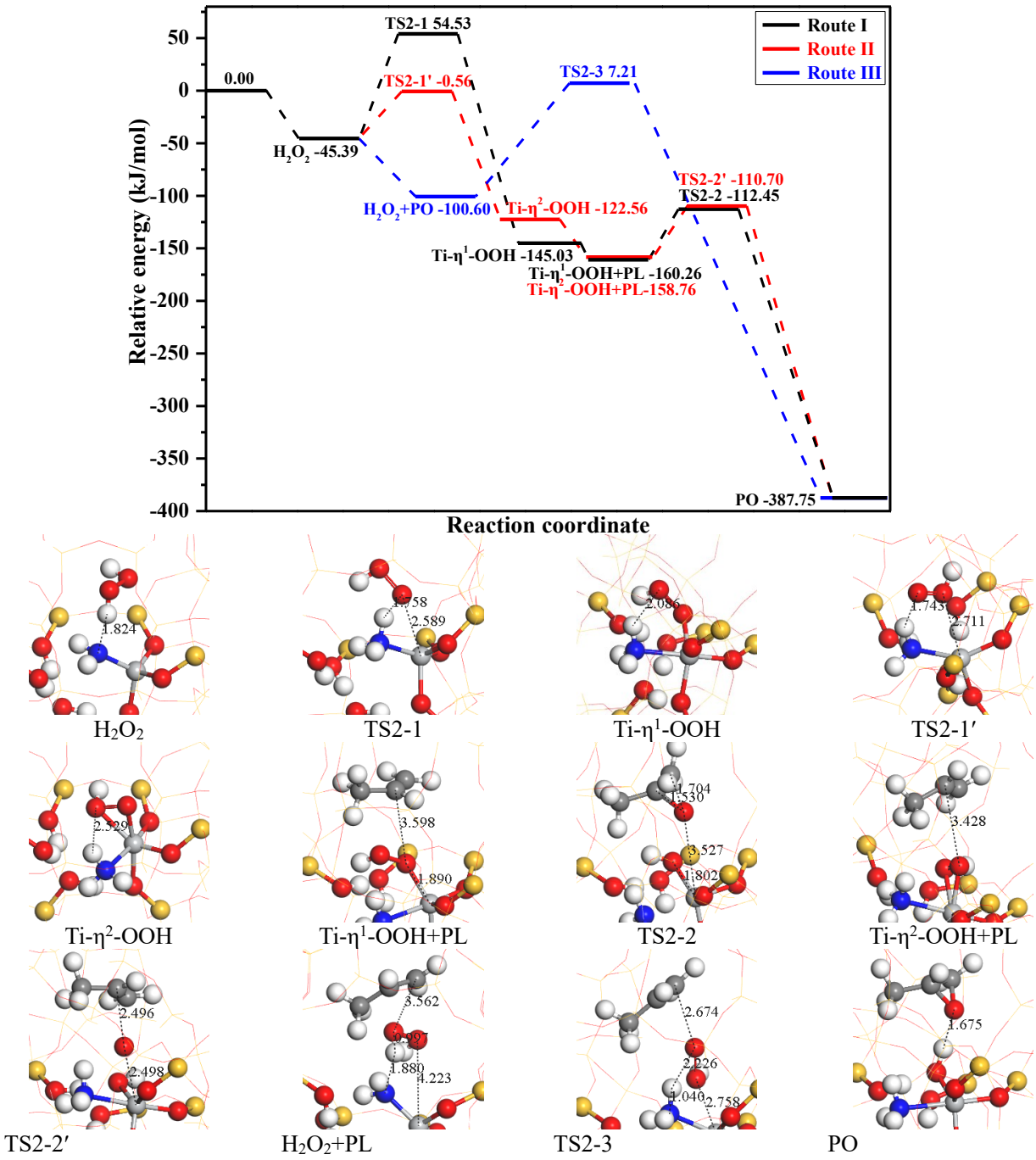

Fig. S4 Relative energy profiles for three routes of propylene epoxidation at the nitrided Ti/defect site at 313 K, together with the structures of reactant, transition state, intermediate and product. Route I, the "two-step" mechanism *via* Ti-η^1-OOH intermediate; Route II, the "two-step" mechanism *via* Ti-η^2-OOH intermediate; Route III, the "one-step" mechanism. The energy unit is in kJ/mol, and bond length is in Å (N = blue, Ti = light grey, C = grey, O = red, Si = yellow and H = white).

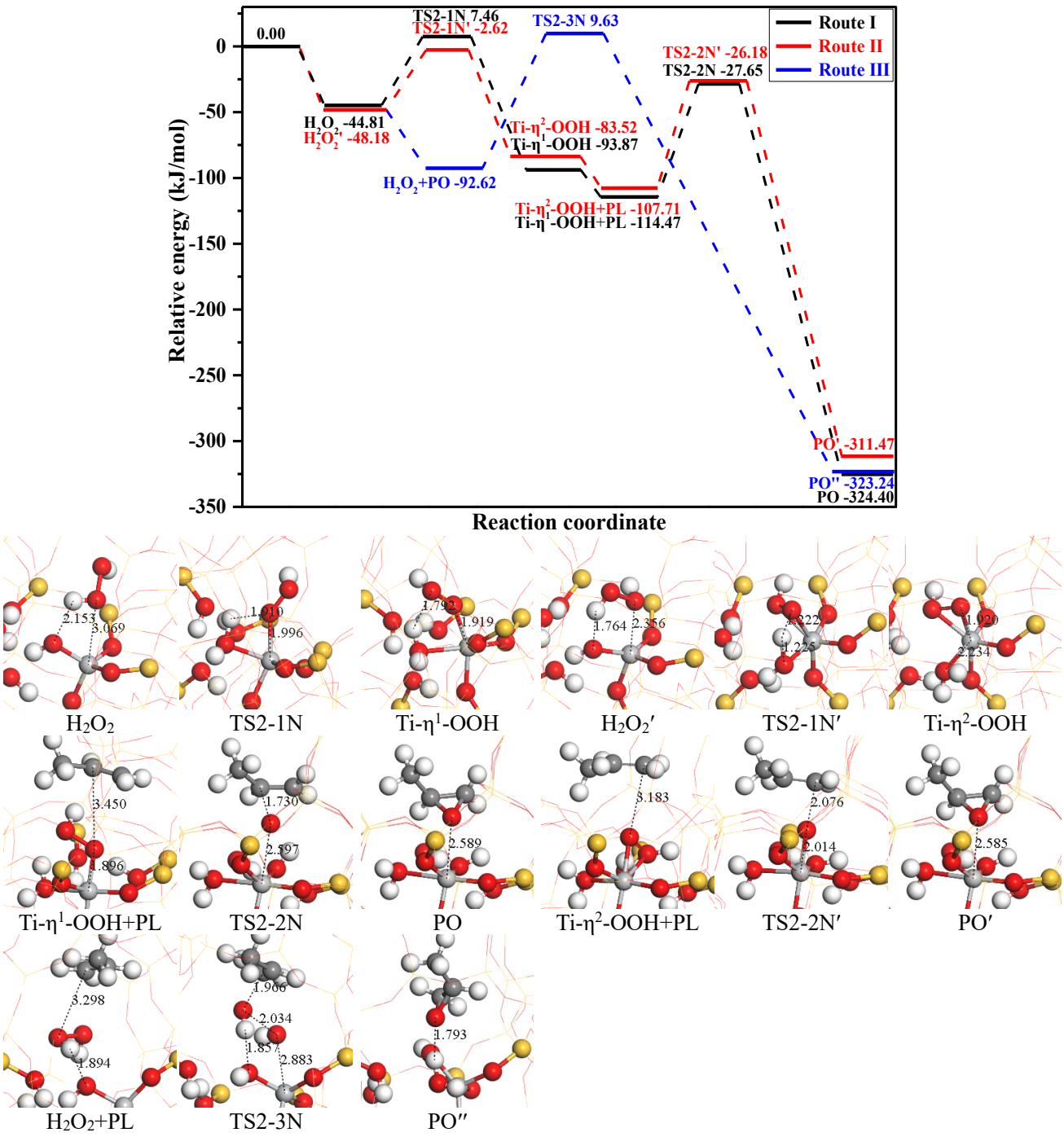

Fig. S5 Relative energy profiles for three routes of propylene epoxidation at the Ti/defect site at 313 K, together with the structures of reactant, transition state, intermediate and product. Route I, the "two-step" mechanism *via* Ti-η^1-OOH intermediate; Route II, the "two-step" mechanism *via* Ti-η^2-OOH intermediate; Route III, the "one-step" mechanism. The energy unit is in kJ/mol, and bond length is in Å. (Ti = light grey, C = grey, O = red, Si = yellow, H = white).

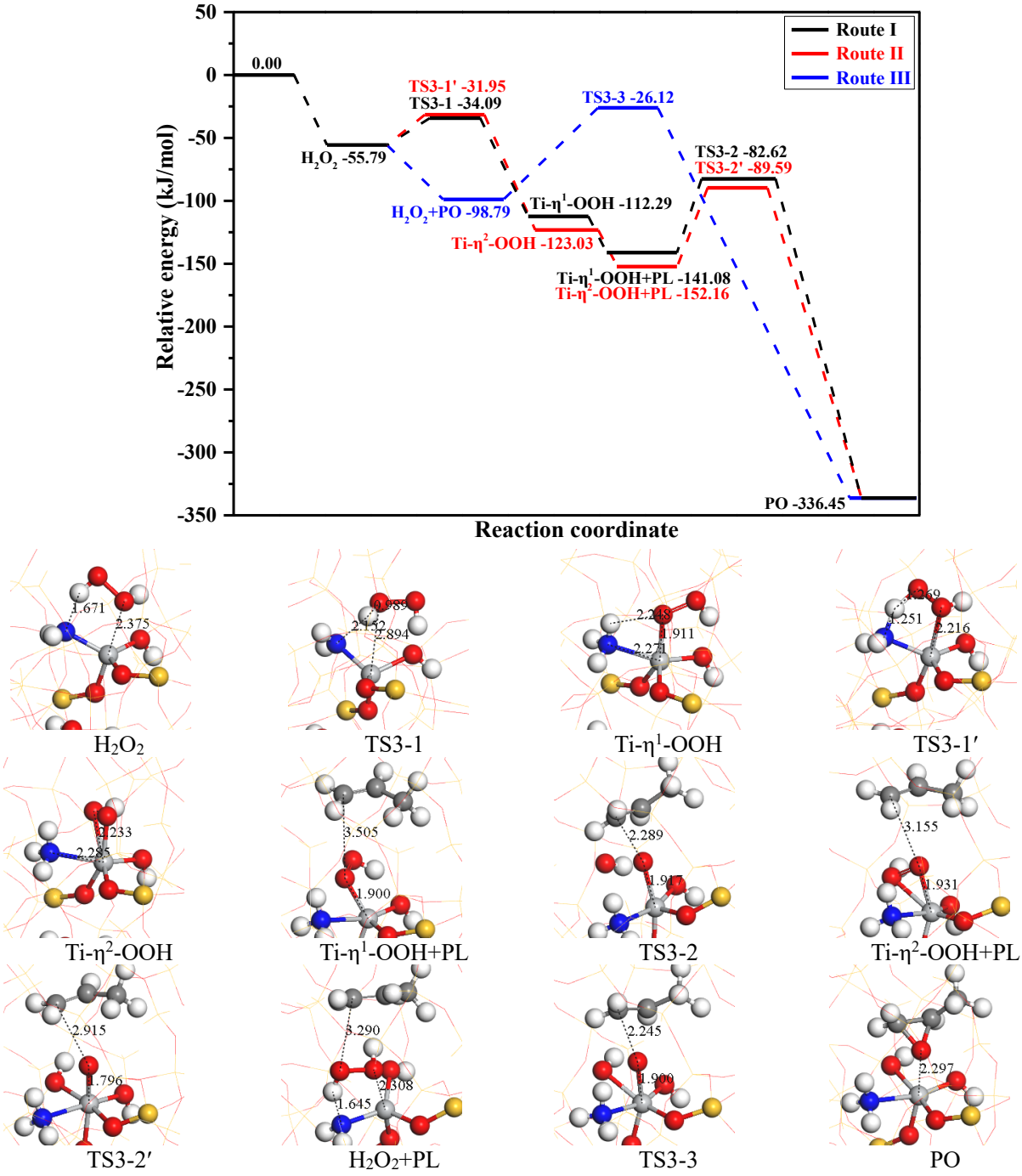

Fig. S6 Relative energy profiles for three routes of propylene epoxidation at nitrided bipodal Ti site at 313 K, together with the structures of reactant, transition state, intermediate and product. Route I, the "two-step" mechanism *via* Ti-η^1-OOH intermediate; Route II, the "two-step" mechanism *via* Ti-η^2-OOH intermediate; Route III, the "one-step" mechanism. The energy unit is in kJ/mol, and bond length is in Å (N = blue, Ti = light grey, C = grey, O = red, Si = yellow and H = white).

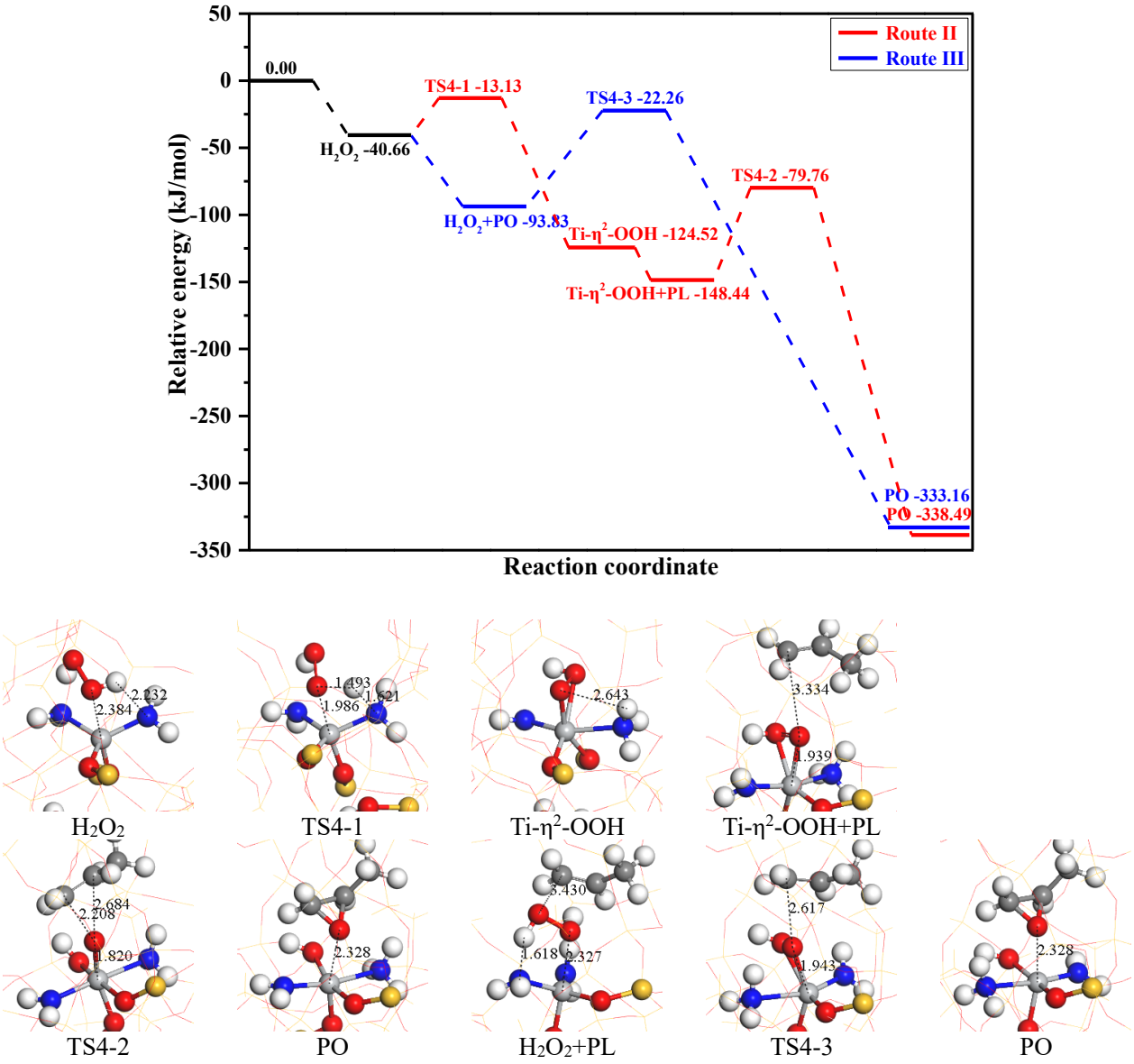

Fig. S7 Relative energy profiles for three routes of propylene epoxidation at the double embedded bipodal Ti site at 313 K, together with the structures of reactant, transition state, intermediate and product. Route II, the "two-step" mechanism *via* Ti-η^2-OOH intermediate; Route III, the "one-step" mechanism. The energy unit is in kJ/mol, and bond length is in Å. (Ti = light grey, C = grey, O = red, Si = yellow, H = white).

S4 Density of States (DOSs) plots of Ti-η^1-OOH at the tetrahedral Ti site, Ti-η^2-OOH at the Ti/defect site and Ti-η^2-OOH on bipodal Ti site

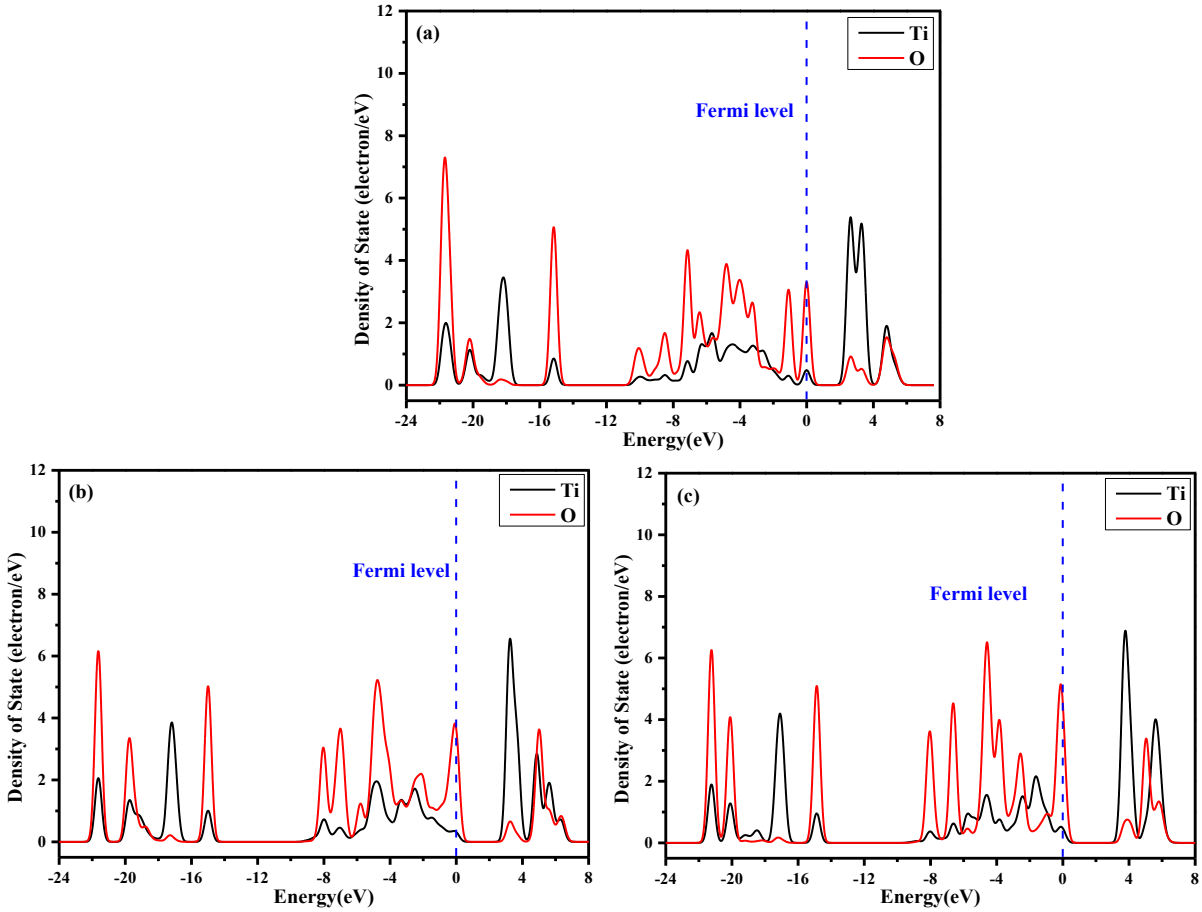

Fig. S8 The density of states (DOSs) plots of (a) Ti-η^1-OOH at the tetrahedral Ti site; (b) Ti-η^2-OOH on the Ti/defect site; (c) Ti-η^2-OOH on the bipodal Ti site.

S5 Potential energy profiles for dissociation of H_2O

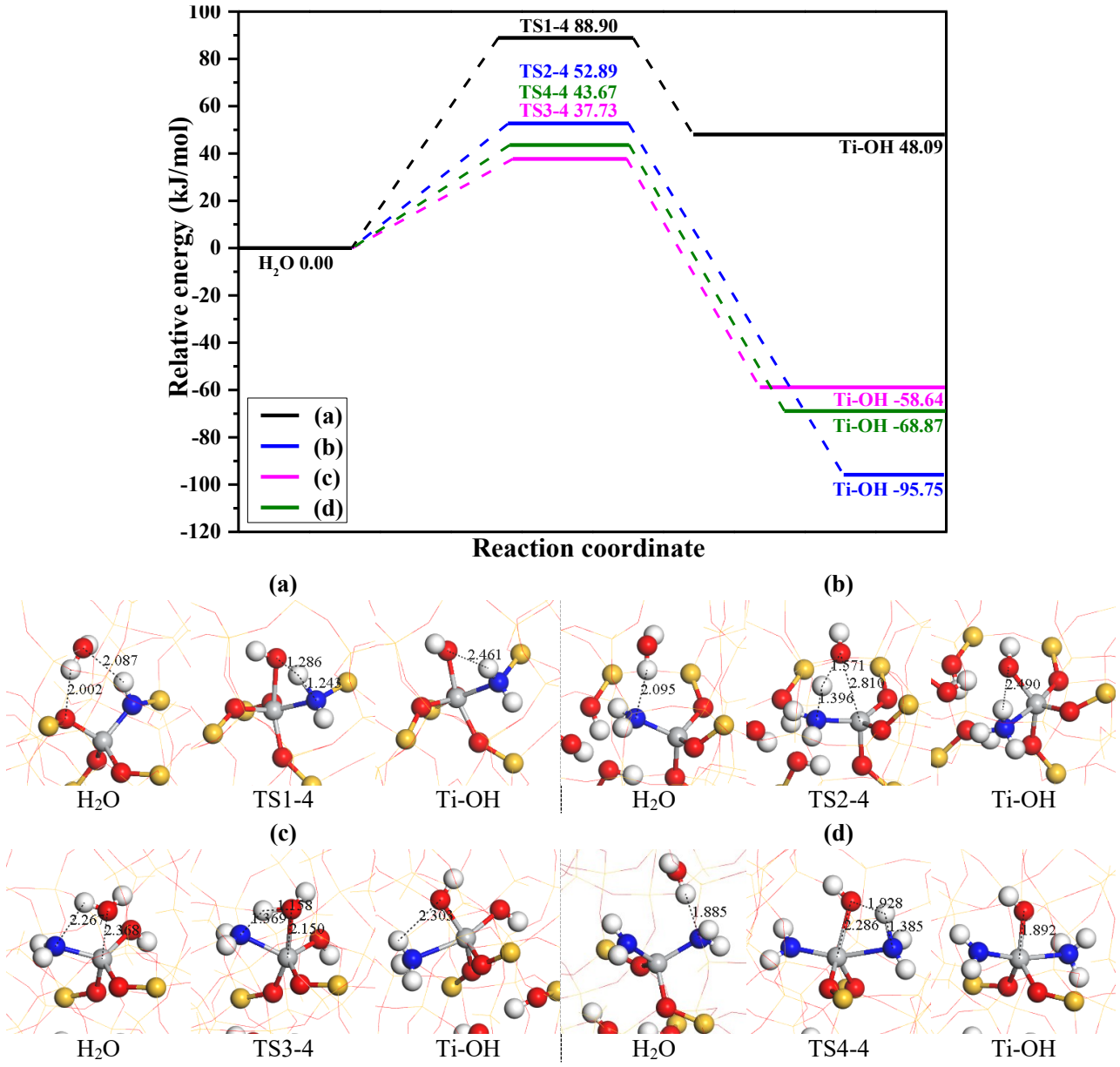

Fig. S9 Potential energy profiles for dissociation of H_2O, together with the structures of reactant, transition state and product at the nitrided (a) tetrahedral Ti, (b) Ti/defect, (c) bipodal Ti and (d) double embedded bipodal Ti sites at 313 K; The bond length is in Å (N = blue, Ti = light grey, C = grey, O = red, Si = yellow and H = white).

In HPPO, the adsorbed H_2O and H_2O_2 may decompose to form the corresponding HO- and HOO- groups, wherein the bond of H-O will break in the adsorbed molecules. The dissociation of H_2O_2 have been investigated in section of propylene epoxidation, therefore, only the dissociation of H_2O is investigated here. At tetrahedral Ti site, the dissociations are initiated by adsorptions of H_2O. Then, the dissociation processed *via* TS1-4, in which the transfer of H to the Ti-NH-Si group occurs concurrently with the formation of the O-Ti bonds. As a result, H_2O dissociated leading to the formation of Ti-NH_2-Si, Ti-OH groups, and the calculated activation free energies and

reaction free energies are 88.90 and 48.09 kJ/mol, correspondingly. Similarly, at Ti/defect and bipodal Ti sites, the dissociations are also initiated by adsorptions of H_2O, and then the transfer of H to the Ti-NH_2 group occurs concurrently with the formation of the O-Ti bonds. As a result, H_2O dissociated leading to the formation of Ti-NH_3 and Ti-OH groups, the calculated activation free energies are 52.89, 37.73 and 43.67 kJ/mol, and correspondingly reaction free energies are -95.75, -58.64 and -68.87 kJ/mol.

S6 Ring-opening of PO with different nucleophiles

Table S3 Mulliken charger (*e*), adsorption free energy (G_{ads}, kJ/mol) and key structural parameter of PO at the different nucleophiles at 313 K and those in parenthesis at 0 K.

Active sites	Nucleophiles	Mulliken charge (*e*)	G_{ads} (kJ/mol)	Adsorption detail	
				Mode	Length (Å)
Tetrahedral Ti site	Ti-N(H)-Si	0.042	-70.96(-49.96)	O…H	1.809
	Ti-OH	0.036	-64.79(-43.60)	O…H	2.278
	Ti-η^1-OOH	0.014	-52.74(-29.05)	O…H	2.135
	Si-N(H)-Si	0.036	-69.44(-49.17)	O…H	1.804
Ti/defect site	Ti-NH_2	0.016	-58.03(-36.31)	O…H	1.900
	Ti-OH	0.052	-39.36(-19.43)	O…H	1.675
	Ti-η^1-OOH	0.015	-39.81(-21.80)	O…H	1.702
	Ti-η^2-OOH	0.015	-68.12(-47.80)	O…H	2.526
	Si-NH_2	0.005	-56.46(-32.05)	O…H	2.111
Bipodal Ti site	Ti-NH_2	0.171	-42.97(-32.50)	O…Ti	2.244
	Ti-OH	0.033	-40.72(-30.17)	O…H	1.749
	Ti-OH′	0.123	-44.08(-33.52)	O…Ti	2.411
	Ti-η^1-OOH	0.017	-46.24(-27.96)	O…H	2.056
	Ti-η^2-OOH	0.054	-48.67(-34.95)	O…H	1.680
Double embedded bipodal Ti site	Ti-NH_2	0.027	-39.03(-23.60)	O…H	1.859
	Ti-OH	0.017	-47.49(-30.52)	O…H	1.871
	Ti-OH′	0.131	-42.26(-28.69)	O…H	2.328
	Ti-η^2-OOH	0.059	-30.59(-17.14)	O…H	1.626

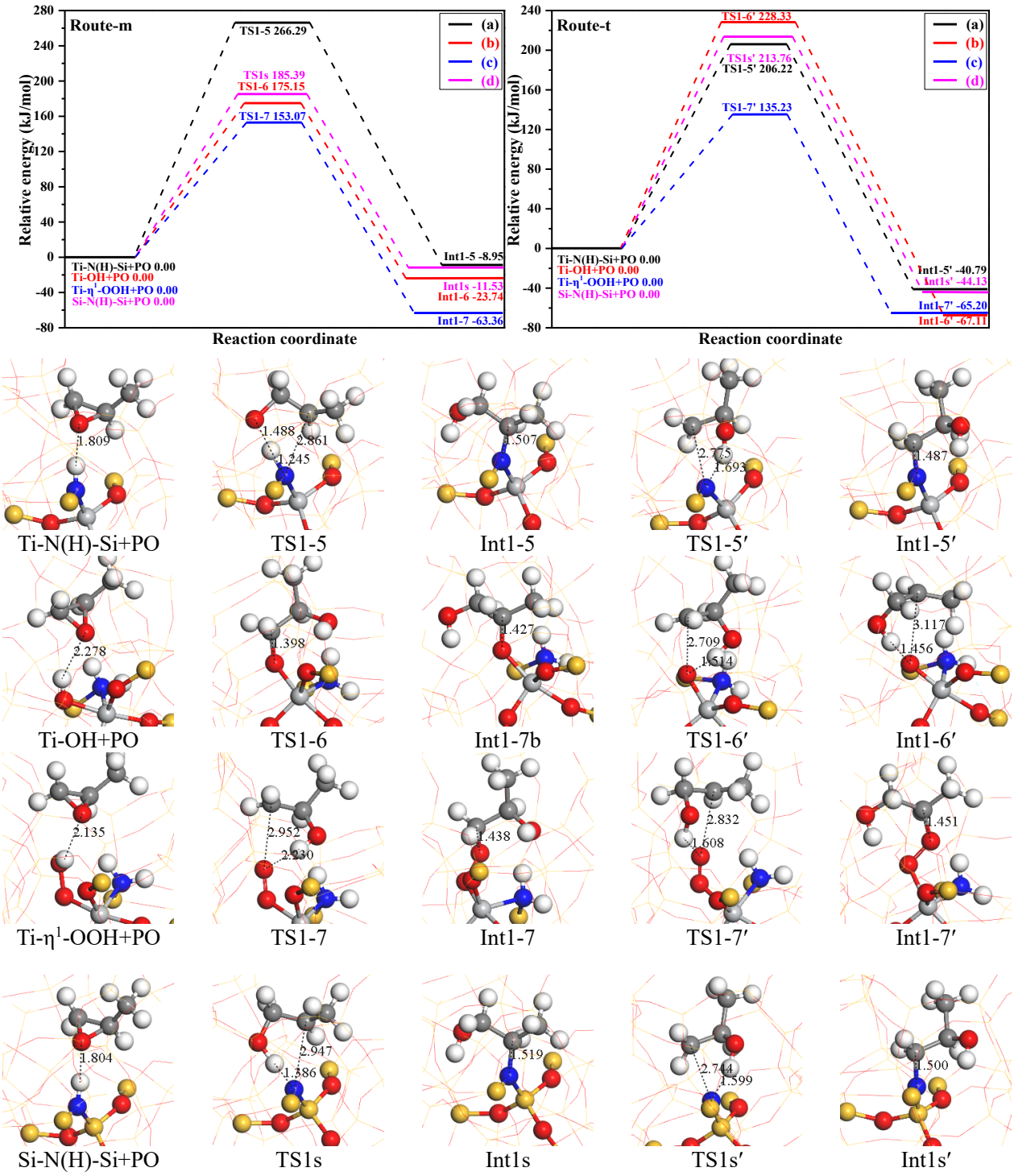

Fig. S10 Potential energy profiles of ring-opening of PO with (a) Ti-N(H)-Si, (b) Ti-OH, (c) Ti-η^1-OOH and (d) Si-N(H)-Si, as well as the structures of reactant, transition state and product at the nitrided tetrahedral Ti site at 313 K; The bond length is in Å (N = blue, Ti = light grey, C = grey, O = red, Si = yellow and H = white).

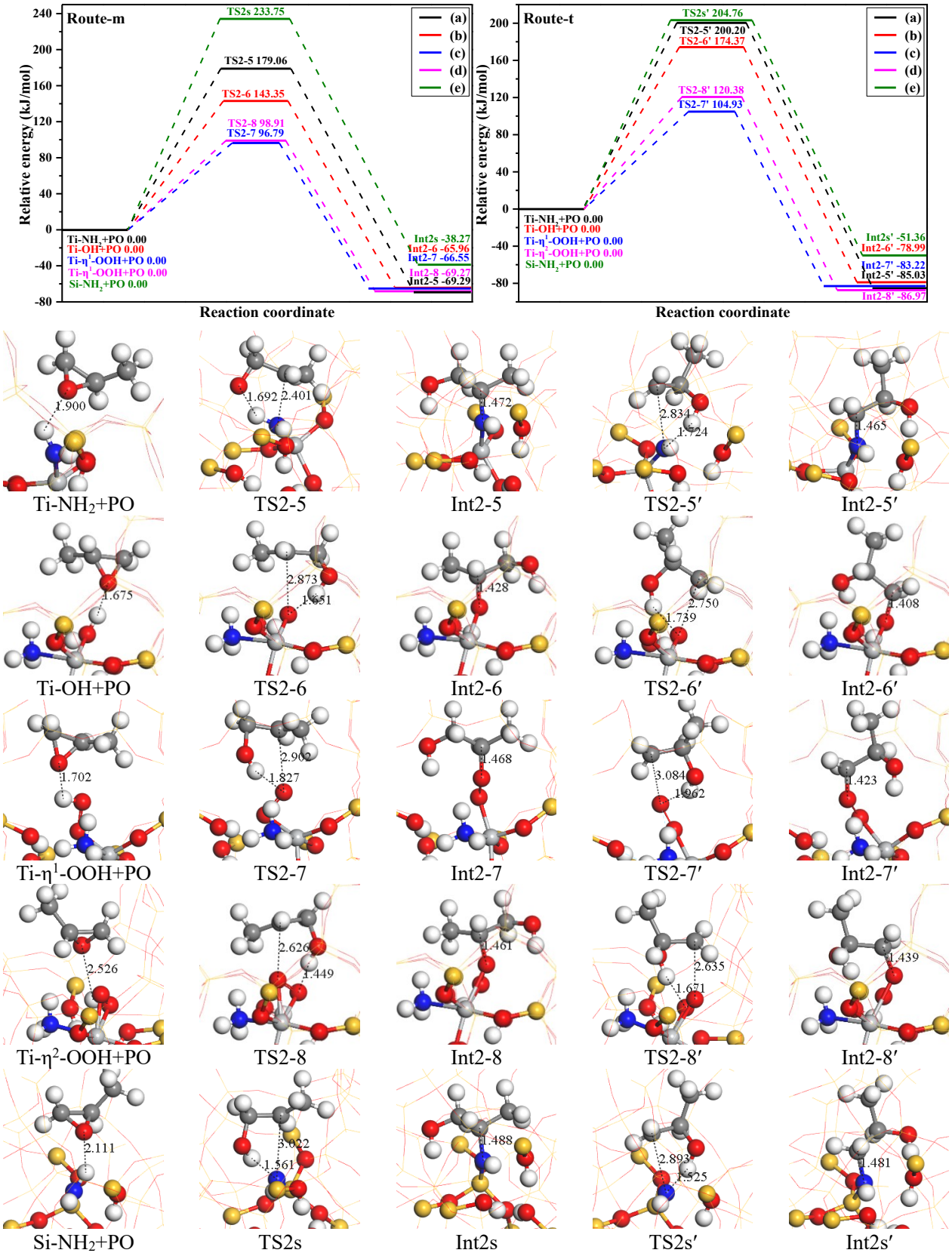

Fig. S11 Potential energy profiles of ring-opening of PO with (a) Ti-NH_2, (b) Ti-OH, (c) Ti-η^1-OOH, (d) Ti-η^2-OOH and (e) Si-NH_2, as well as the structures of reactant, transition state and product at the nitrided Ti/defect site at 313 K; The bond length is in Å (N = blue, Ti = light grey, C = grey, O = red, Si = yellow and H = white).

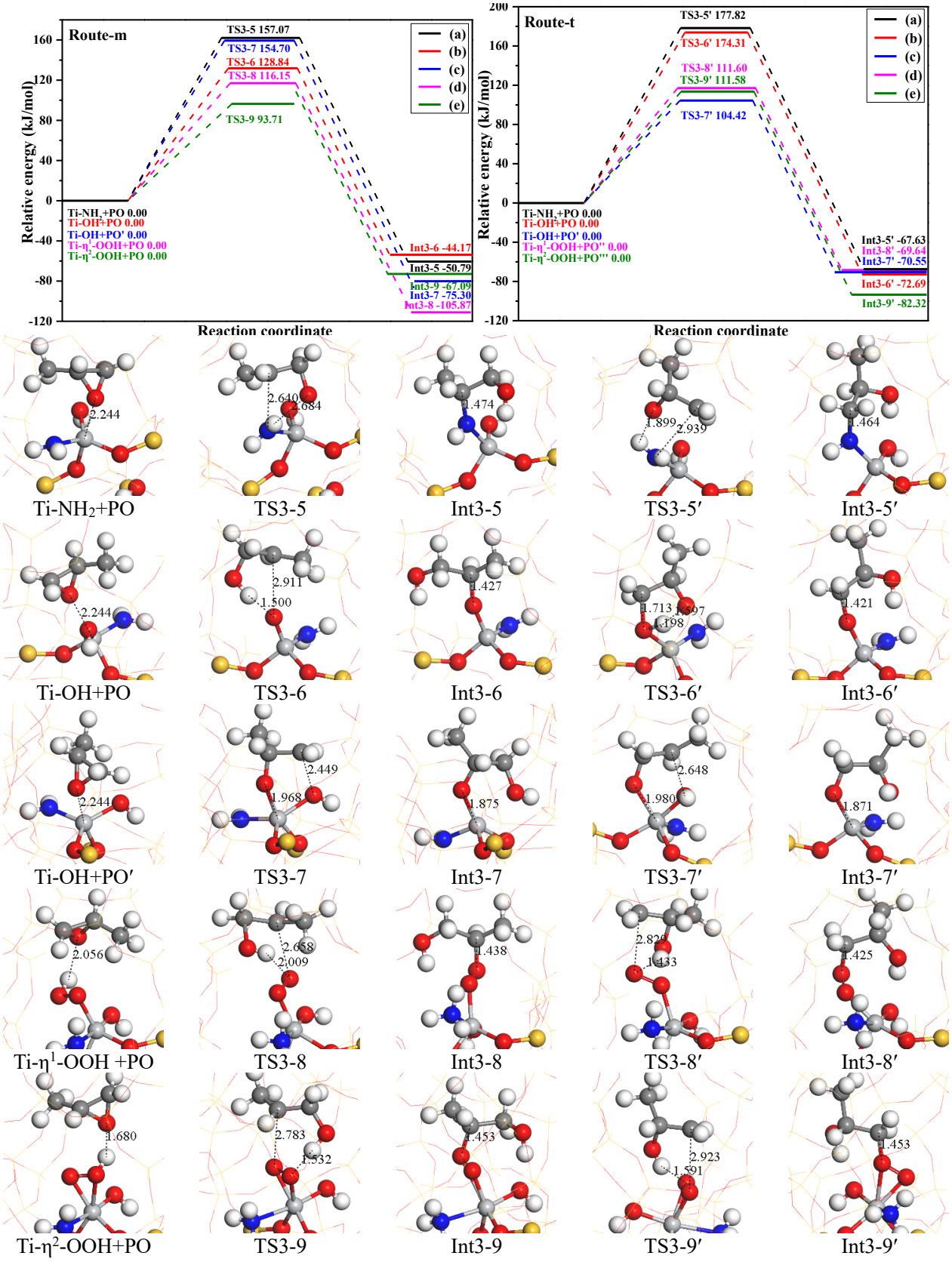

Fig. S12 Potential energy profiles of ring-opening of PO with (a) Ti-NH_2, (b c) Ti-OH, (d) Ti-η^1-OOH and (e) Ti-η^2-OOH, as well as the structures of reactant, transition state and product at the nitrided bipodal Ti site at 313 K; The bond length is in Å (N = blue, Ti = light grey, C = grey, O = red, Si = yellow and H = white).

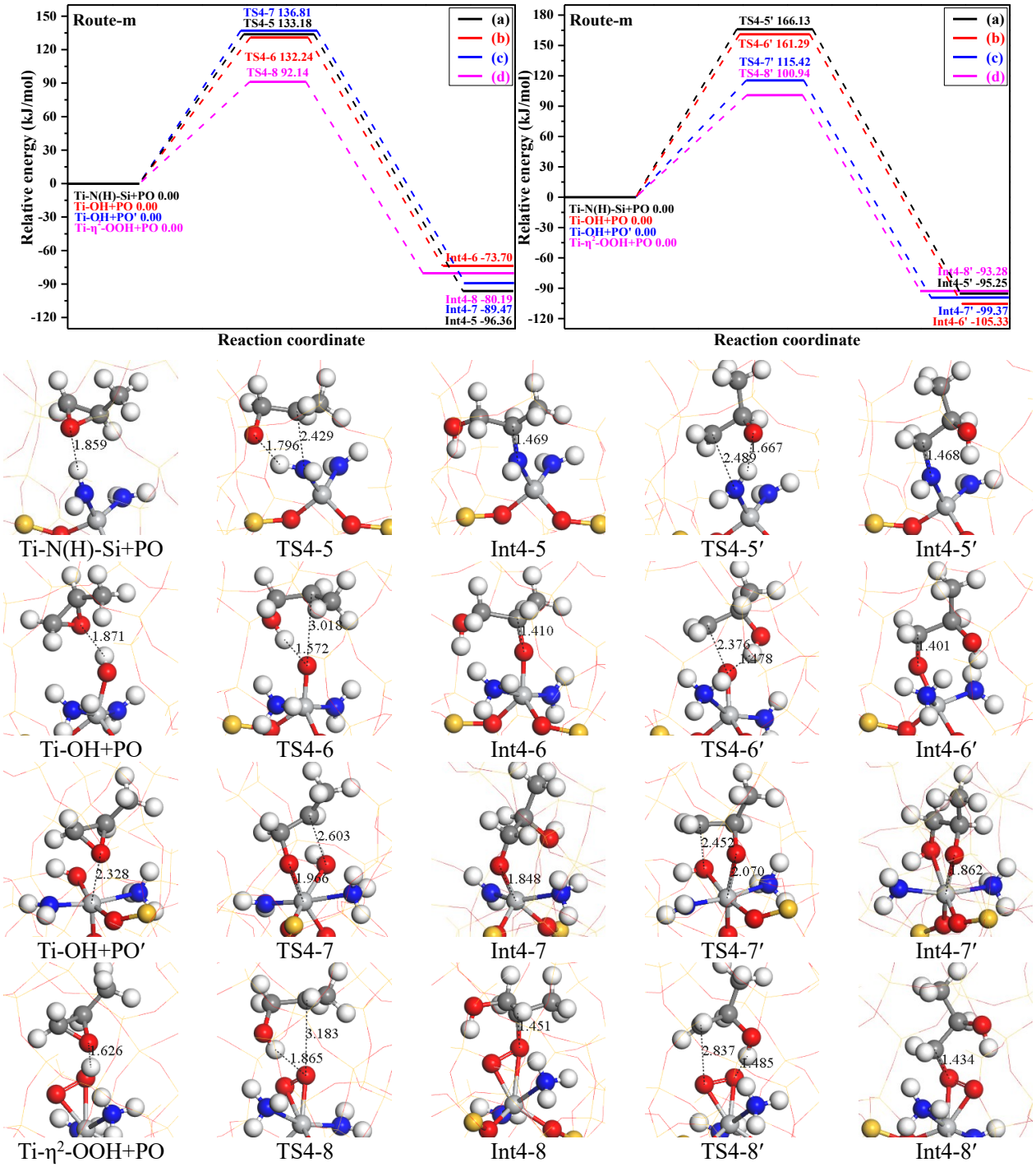

Fig. S13 Potential energy profiles of ring-opening of PO with (a) Ti-N(H)-Si, (b~c) Ti-OH and (d) Ti-η^2-OOH, as well as the structures of reactant, transition state and product at the nitrided double embedded bipodal Ti site at 313 K; The bond length is in Å (N = blue, Ti = light grey, C = grey, O = red, Si = yellow and H = white).

S7 Formation of by-products

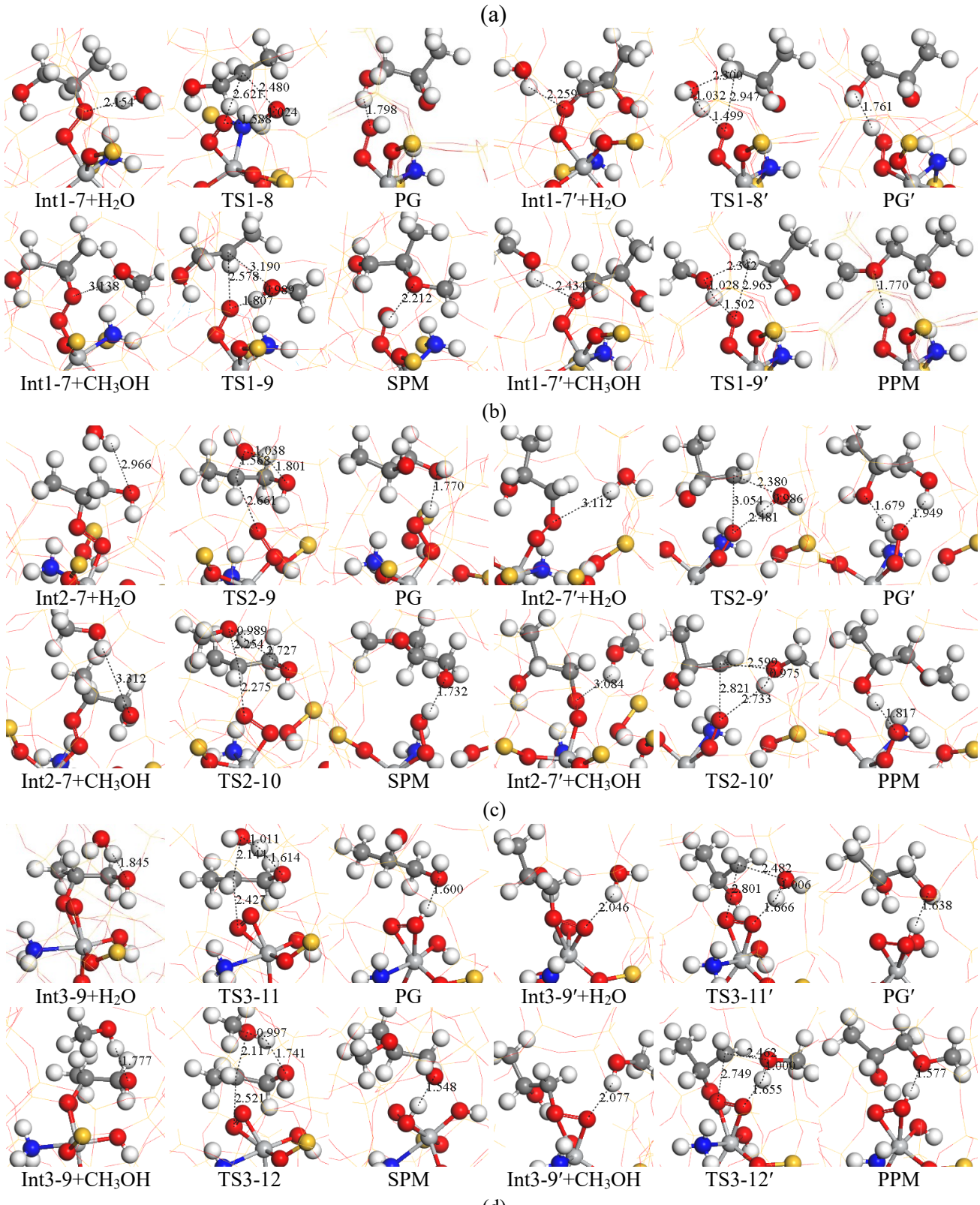

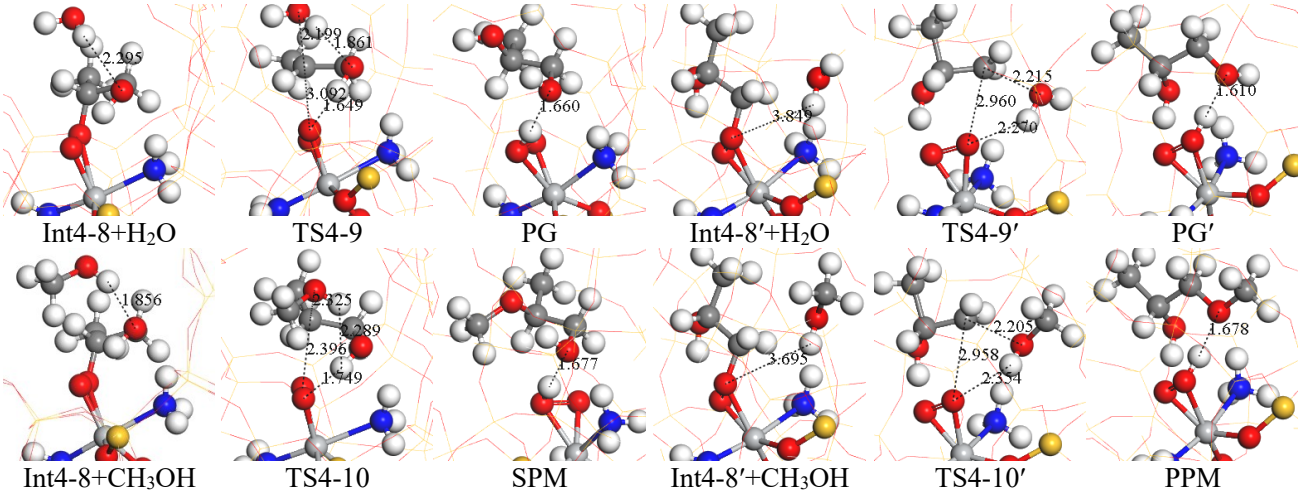

Fig. S14 Structures of reactant, transition state and product for PG, SPM and PPM formation *via* "two-step" mechanism at the nitrided (a) tetrahedral Ti, (b) Ti/defect, (c) bipodal Ti and (d) double embedded bipodal Ti sites at 313 K; The bond length is in Å (N = blue, Ti = light grey, C = grey, O = red, Si = yellow and H = white).

The potential energy diagrams of the entire reaction path for the formation of PG, SPM and PPM through the "two-step" mechanism

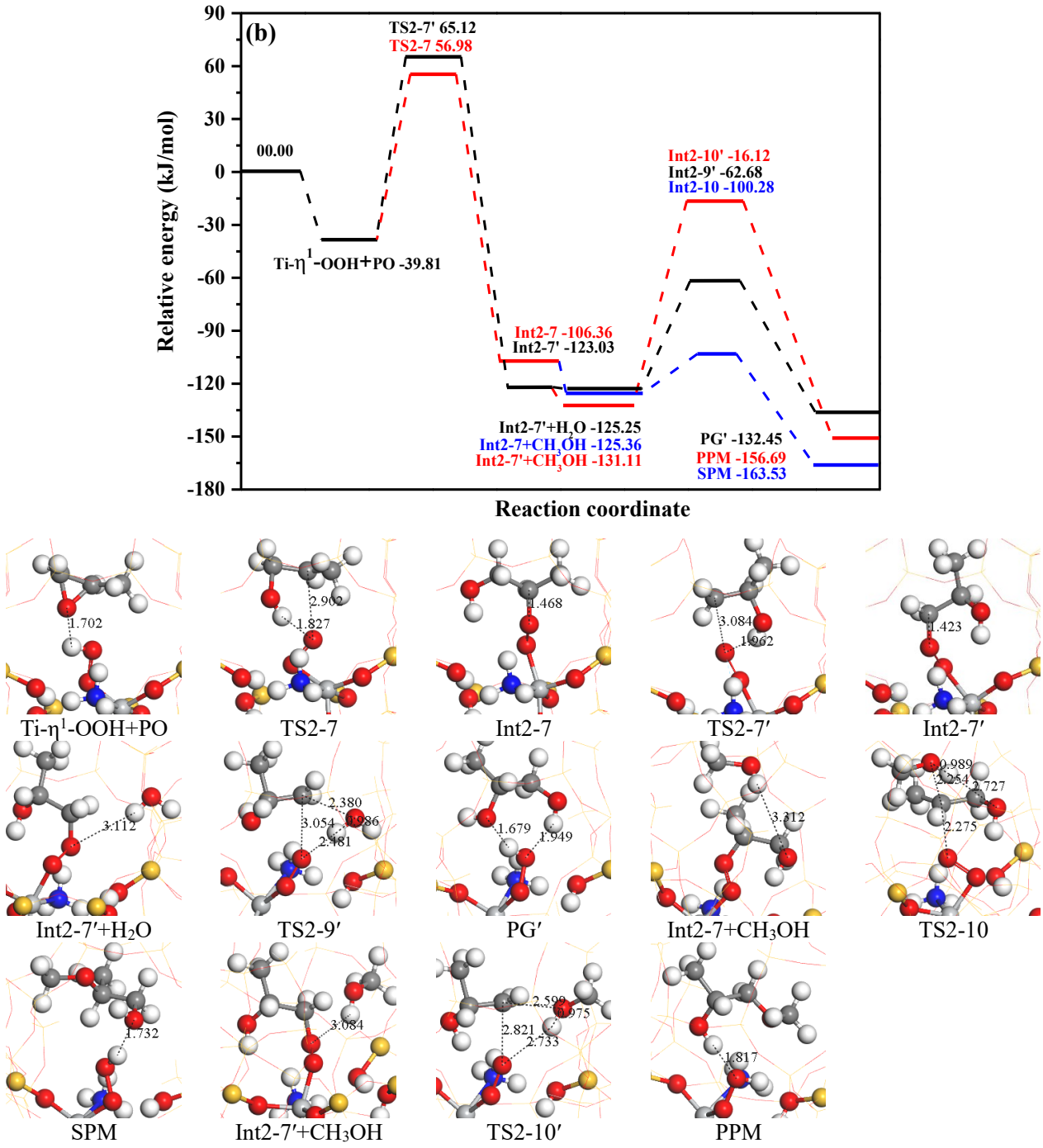

Fig. S15 Relative energy profiles of optimal paths of PG, PPM and SPM formation *via* "two-step" mechanism at the nitrided Ti/defect site at 313 K; The bond length is in Å (N = blue, Ti = light grey, C = grey, O = red, Si = yellow and H = white).

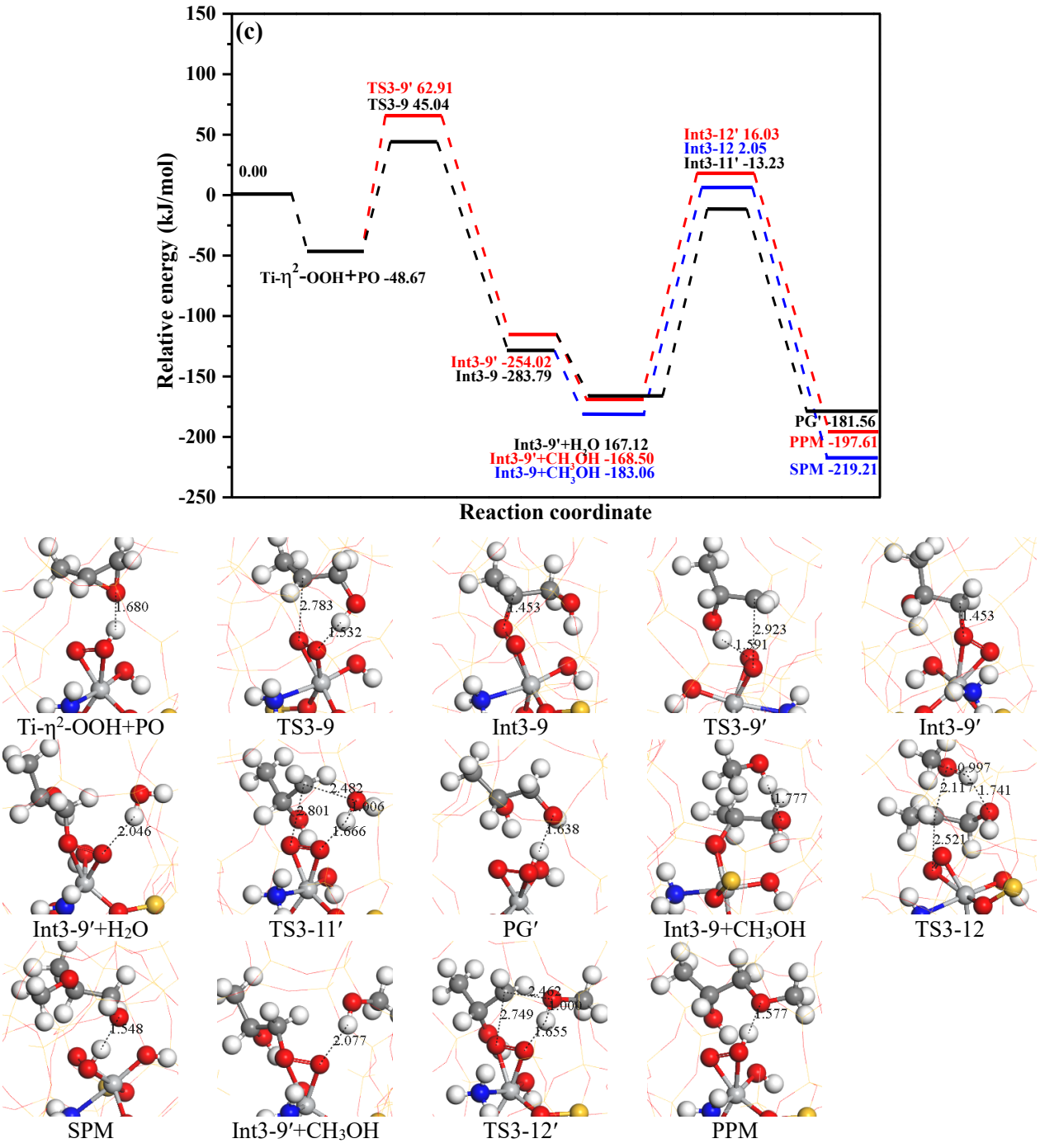

Fig. S16 Relative energy profiles of optimal paths of PG, PPM and SPM formation *via* "two-step" mechanism at the nitrided bipodal Ti site at 313 K; The bond length is in Å (N = blue, Ti = light grey, C = grey, O = red, Si = yellow and H = white).

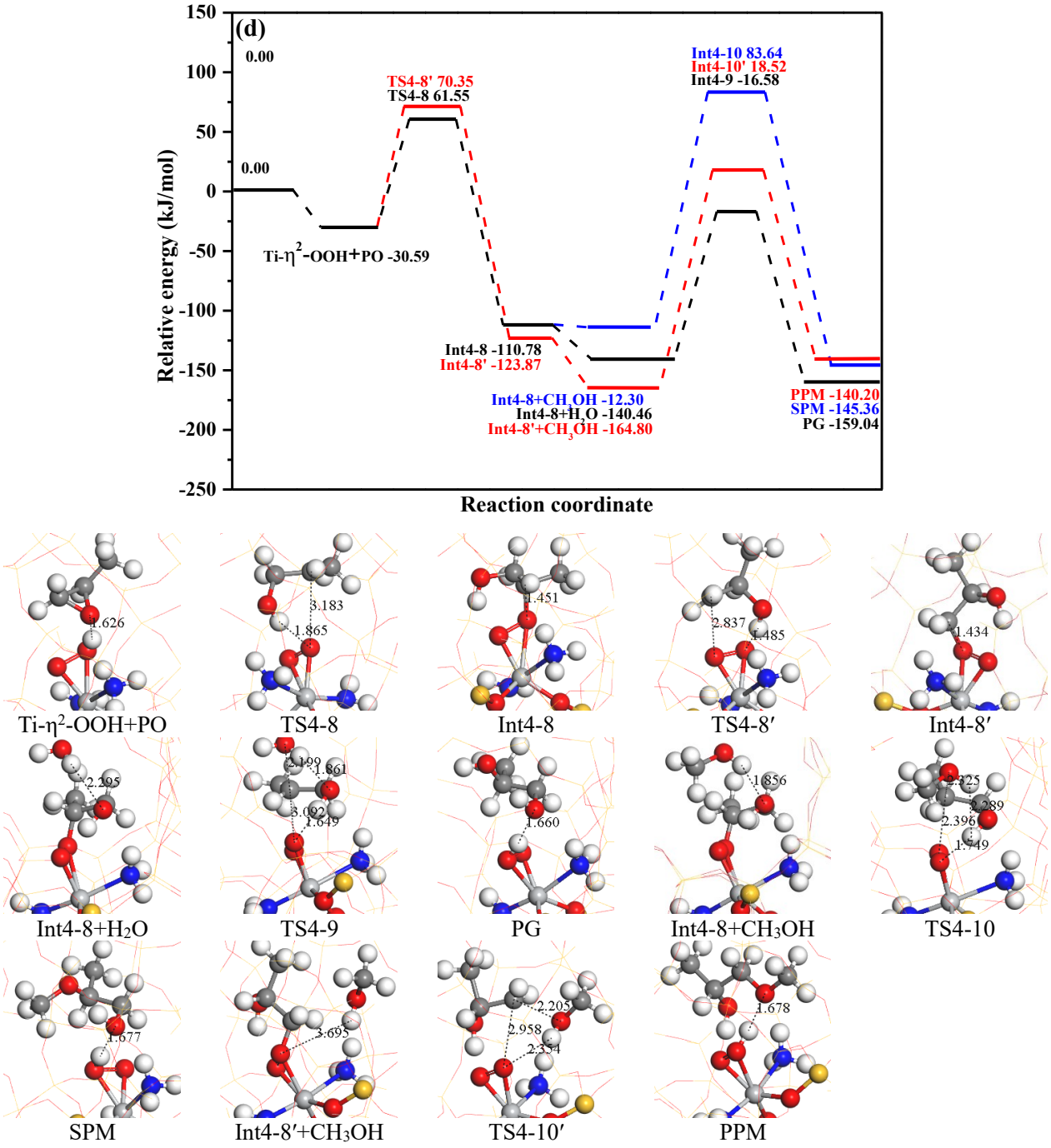

Fig. S17 Relative energy profiles of optimal paths of PG, PPM and SPM formation *via* "two-step" mechanism at the nitrided double embedded bipodal Ti site at 313 K; The bond length is in Å (N = blue, Ti = light grey, C = grey, O = red, Si = yellow and H = white).

The potential energy diagrams of the entire reaction path for the formation of PG, SPM and PPM through the "one-step" mechanism

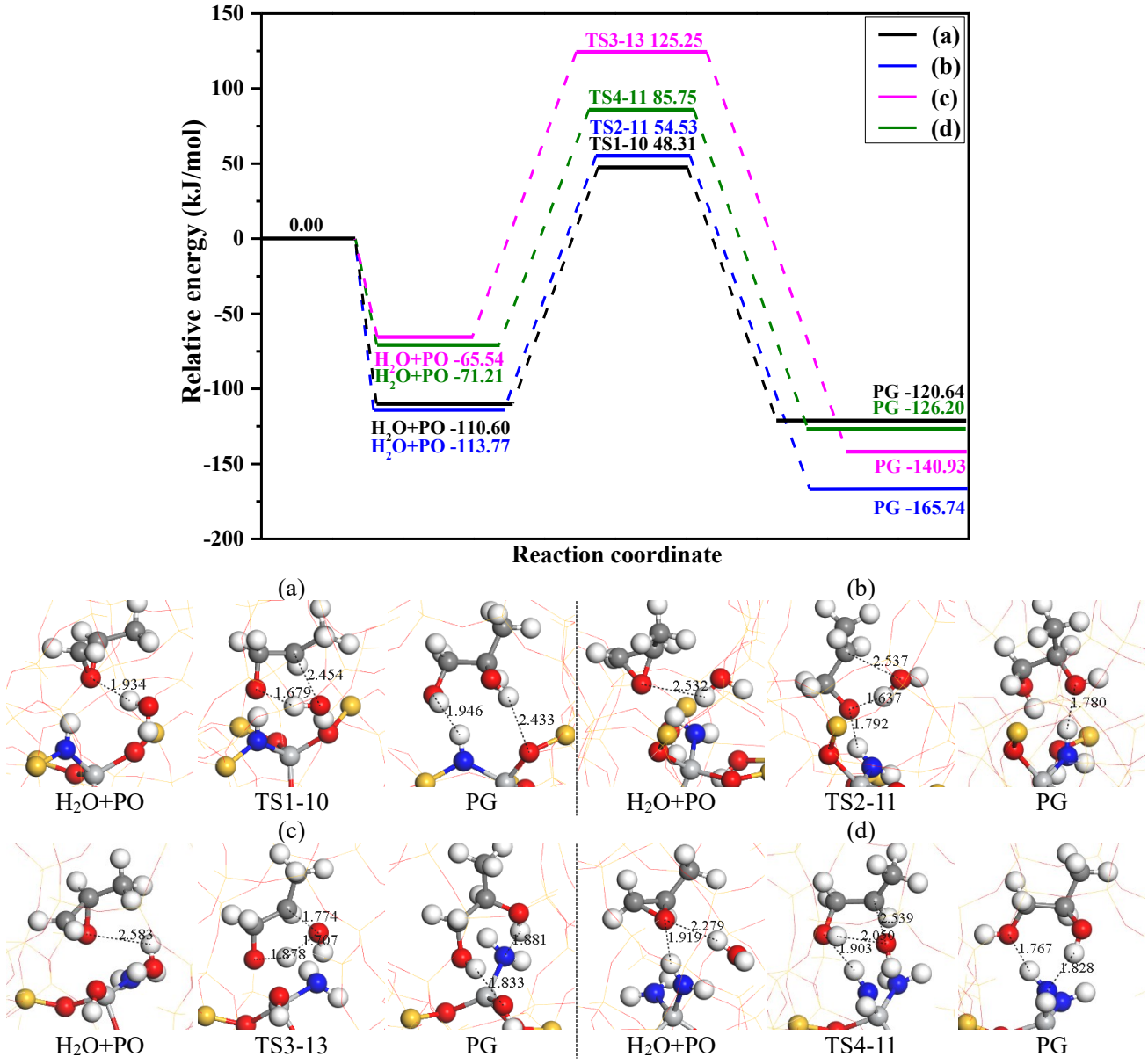

Fig. S18 Potential energy profiles of PG formation *via* "one-step" reaction mechanism, together with the structures of reactant, transition state and product at the nitrided (a) tetrahedral Ti, (b) Ti/defect, (c) bipodal Ti and (d) double embedded bipodal Ti sites at 313 K; The bond length is in Å (N = blue, Ti = light grey, C = grey, O = red, Si = yellow and H = white).

Fig. S18 shows the potential energy diagrams of PG generated by "one-step" mechanism and the structures of the corresponding reactants, transition states and products. The obtained activation free energies are 158.91, 176.87, 168.30, 190.79 and 156.96 kJ/mol, respectively, and the corresponding reaction free energies are -10.04, -60.76, -51.97, -75.39 and -54.99 kJ/mol.

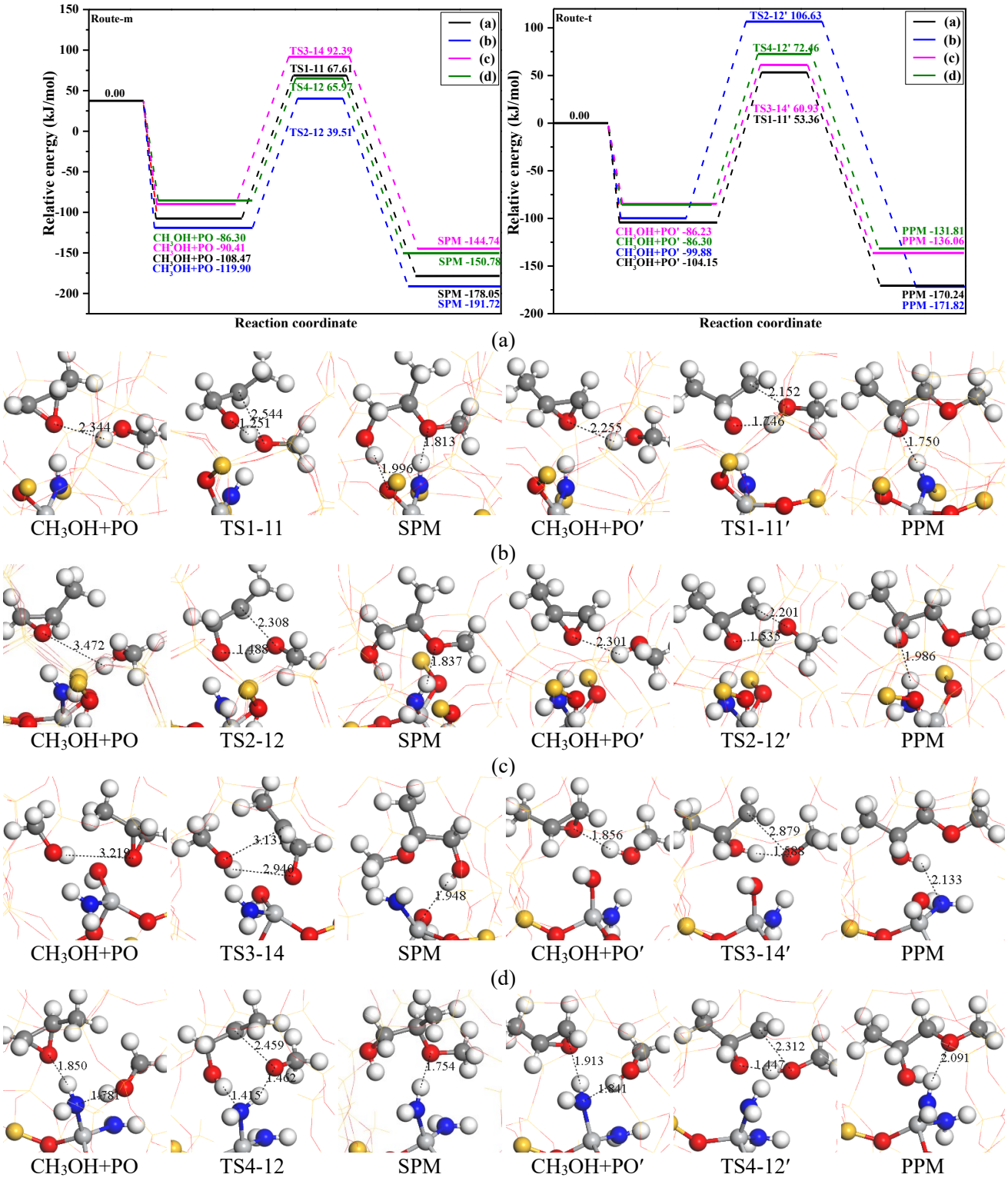

Fig. S19 Potential energy profiles of SPM and PPM formations *via* "one-step" mechanism, together with the structures of reactant, transition state and product on nitrided (a) tetrahedral Ti, (b) Ti/defect, (c) bipodal Ti and (d) double embedded bipodal Ti sites at 313 K; The bond length is in Å (N = blue, Ti = light grey, C = grey, O = red, Si = yellow and H = white).

Fig. S19 show the potential energy diagrams of SPM and PPM generated by “one-step” mechanism and the structures of the corresponding reactants, transition states and products. The activation free energy barriers that need to be overcome to form SPM are 176.08, 205.85, 159.41, 182.8 and 152.27 kJ/mol, respectively, and the corresponding reaction free energies are -69.58, -56.14, -71.82, -54.33 and -64.48 kJ/mol. The activation free energy and reaction free energy obtained for PPM formation are 157.51, 187.57, 206.51, 147.16, 158.76 kJ/mol and -66.09, -48.12, -71.94, -49.83, -45.51 kJ/mol, respectively. Comparing the total activation free energy barriers of two reaction mechanisms to generate PG, SPM and PPM, it can be determined that except for the coexistence of “one-step” and “two-step” reaction mechanism for PG reaction at nitrided tetrahedral Ti site, the other active centers pass through “two-step” mechanism are more favorable.

S8 Calculation of thermodynamic parameters and microkinetic analysis of propylene epoxidation

Adsorption free energy, activation free energy and reaction free energy were calculated using the following formulas:

$$G_{ads}=E_{(adsorbate/catalyst)}-E_{(catalyst)}-E_{(adsorbate)}+\Delta G_{ads} \quad (1)$$

$$\Delta G_{ads}=G_{(adsorbate/catalyst)}-G_{(catalyst)}-G_{(adsorbate)} \quad (2)$$

$$G_a=E_{TS}-E_R+\Delta G_a \quad (3)$$

$$\Delta G=E_P-E_R+\Delta G_H \quad (4)$$

$$\Delta G_a=G_{TS}-G_R \quad (5)$$

$$\Delta G_H=G_P-G_R \quad (6)$$

Where $E_{(adsorbate/catalyst)}$, $E_{(adsorbate)}$ and $E_{(catalyst)}$ are the total energy of re the total energies of the adsorbate-catalyst complex, catalyst, and adsorbate, respectively. E_R, E_{TS} and E_P are the total energies of reactant, transition state and final state in an elementary reaction, respectively. G_R, G_{TS} and G_P are the Gibbs free energy corrections of reactant, transition state and final state, respectively. Considering the contributions of thermal energy and entropy to the standard molar Gibbs free energy, the standard molar Gibbs free energy can be obtained using following formula.[11-13]

$$G=E_{total}+E_{ZPE}+U-TS+\gamma RT \quad (7)$$

$$E_{ZPE}=\sum_i \frac{h\nu_i}{2} \quad (8)$$

$$U_{Vib}=RT\sum_i \frac{h\nu_i/k_BT}{e^{h\nu_i/k_BT}-1} \quad (9)$$

$$S=R\sum_{i=1}^{n}-\ln\left(1-e^{h\nu_i/k_BT}\right)+\frac{h\nu_i/k_BT}{e^{h\nu_i/k_BT}-1} \quad (10)$$

Where E_{total} is the QM/MM total energy, R is the gas constant, γ = 0 for adsorbed species and 1 for isolated molecules, k_B is the Boltzmann constant, and T is the reaction temperature (313~333 K); R is the gas constant, and γ is 0 for adsorbed species, and 1 for isolated molecule; is the Boltzmann constant, T is the actual temperature. All the calculation results are summarized in Table S7-S10.

With respect of "one-step" mechanism for propylene epoxidation, the adsorptions of H_2O_2, CH_3OH, C_3H_6 and H_2O are presumed to represent equilibrium, in which equilibrium coverage determined as function of reactant mole ratios, and assuming competitive Langmuir adsorption and excluding possible other adsorbed species, such as PO.

The coverages are calculated by the following formulas:

$$\theta_{H_2O_2} = \frac{K_{H_2O_2}[H_2O_2]}{1+K_{H_2O_2}[H_2O_2]+K_{C_3H_6}[C_3H_6]+K_{H_2O}[H_2O]+K_{CH_3OH}[CH_3OH]} \quad (11)$$

$$\theta_{C_3H_6} = \frac{K_{C_3H_6}[C_3H_6]}{1+K_{H_2O_2}[H_2O_2]+K_{C_3H_6}[C_3H_6]+K_{H_2O}[H_2O]+K_{CH_3OH}[CH_3OH]} \quad (12)$$

The equilibrium constants for H_2O_2, CH_3OH, C_3H_6 and H_2O adsorption are estimated by the formula [14]:

$$K = \exp[-\frac{E_{ads}-T\Delta S}{k_B T}] \quad (13)$$

E_{ads} are the adsorption free energies of H_2O_2, CH_3OH, C_3H_6 and H_2O, k_B is the Boltzmann constant, T is the reaction temperature (313 K) and ΔS are the entropy changes of H_2O_2, CH_3OH, C_3H_6 and H_2O, which are obtained from NIST Chemistry WebBook. The reaction rate constants (k) can be obtained using harmonic transition state theory:[14]

$$k = \frac{k_B T}{h}\frac{q_{TS}}{q_R}\exp(-\frac{E_{act}}{k_B T}) \quad (14)$$

$$q = \frac{1}{\prod_{i=1}^{Vibration} 1-\exp(-\frac{h\nu_i}{k_B T})} \quad (15)$$

Where k_B is the Boltzmann constant, T is the actual temperature (350 K), and E_{act} represents the zero-point-corrected activation free energy.

The reaction rate *via* "one-step" mechanism for PO formation is calculated by:

$$r_3 = k_3\theta_{H_2O_2}\theta_{C_3H_6} \quad (16)$$

Under the experimental conditions, all reaction conditions at 313 K; the reactant mole ratios of [H_2O_2], [CH_3OH], [H_2O] in microkinetic analysis are 0.1, 0.5 and 0.4, correspondingly; the [C_3H_6] is 0.4 Mpa.[15.]

For the "two-step" mechanism, we first considered H_2O_2 adsorption and dissociation due to propylene epoxidation involves Ti-η^1-OOH or Ti-η^2-OOH intermediates. The reactions of Ti-η^1-OOH or Ti-η^2-OOH formation are supposed to be equilibrium. The step of produce PO is described by the forward rate. The site balance of intermediate species (Ti-η^1-OOH or Ti-η^2-OOH, intermediate of favorable paths is selected) included in the reaction mechanism can be written in terms of coverage ($\theta_{Ti\text{-}OOH}$).

$$\theta_{H_2O_2} + \theta_{Ti\text{-}OOH} + \theta_{H_2O} + \theta_{CH_3OH} + \theta^* = 1 \quad (17)$$

The θ^* is the coverage of vacancy. The coverage of H_2O_2, H_2O, CH_3OH, and Ti-OOH is calculated as follows:

$$\theta_{H_2O_2} = K_{H_2O_2}[H_2O_2]\theta^* \quad (18)$$

$$\theta_{H_2O} = K_{H_2O}[H_2O]\theta^* \quad (19)$$

$$\theta_{CH_3OH} = K_{CH_3OH}[CH_3OH]\theta^* \quad (20)$$

$$\theta_{Ti\text{-}OOH} = k_1\theta_{H_2O_2}\theta^* \quad (21)$$

By putting equations (18) (19) (20) and (21) into (17), we can calculate θ^* and coverage of other species according to the equilibrium-state approximation presented as follows:

$$K_{H_2O_2}[H_2O_2]\theta^* + k_1\theta_{H_2O_2}\theta^*\theta^* + K_{H_2O}[H_2O]\theta^* + K_{CH_3OH}[CH_3OH]\theta^* + \theta^* = 1 \quad (22)$$

According to these equations, we can obtain the result of $\theta_{Ti\text{-}OOH}$. Therefore, the epoxidation reaction rate *via* "two-step" mechanism can be calculated by:

$$r_2 = k_2\theta_{Ti\text{-}OOH}[C_3H_6] \quad (23)$$

All equilibrium constants of H_2O_2, CH_3OH, H_2O and C_3H_6 adsorption (K) and the rate constants k (s^{-1}) of PL→PO *via* "one-step" and "two-step" mechanism used for calculation are summarized in Table S1.

Table S4 The equilibrium constants of H_2O_2, CH_3OH, H_2O and C_3H_6 adsorption (K) and the rate constants k (s^{-1}) of the related elementary reaction involved in PL→PO at the nitrided (a) tetrahedral Ti, (b) Ti/defect, (c) bipodal Ti and (d) double embedded bipodal Ti sites (T=313 K).

K/k	(a)	(b)	(c)	(d)
$K_{H_2O_2}$	8.19×10^{7}	6.10×10^{9}	1.40×10^{11}	4.24×10^{8}
K_{CH_3OH}	8.61×10^{10}	4.84×10^{8}	1.76×10^{8}	9.42×10^{9}
K_{H_2O}	9.22×10^{8}	3.71×10^{9}	2.40×10^{7}	1.09×10^{6}
$K_{C_3H_6}$	8.84×10^{8}	7.09×10^{7}	4.97×10^{7}	6.58×10^{8}
k_1	2.06×10^{-1}	6.94×10^{3}	5.58×10^{8}	7.87×10^{7}
k_2	9.49×10^{-2}	2.74×10^{5}	7.87×10^{2}	1.05×10^{1}
k_3	3.50×10^{-2}	2.46×10^{-6}	1.00×10^{0}	2.21×10^{0}

Table S5 The equilibrium constants of H_2O_2, CH_3OH, H_2O and C_3H_6 adsorption (K) and the rate constants k (s^{-1}) of the related elementary reaction involved in PL→PO at the (a) tetrahedral Ti, (b) Ti/defect and (c) bipodal Ti sites (T=313 K).

K/k	(a)	(b)	(c)
$K_{H_2O_2}$	1.64×10^{6}	8.16×10^{9}	1.51×10^{11}
K_{CH_3OH}	3.43×10^{8}	3.53×10^{10}	1.06×10^{12}
K_{H_2O}	8.73×10^{5}	6.87×10^{9}	5.59×10^{8}
$K_{C_3H_6}$	4.70×10^{7}	4.89×10^{6}	1.59×10^{10}
k_1	3.12×10^{-8}	1.69×10^{5}	6.67×10^{5}
k_2	6.13×10^{-6}	1.78×10^{-1}	4.60×10^{10}
k_3	2.71×10^{-7}	2.04×10^{-5}	1.33×10^{1}

Table S6 The surface coverage of key intermediate species ($\theta_{Ti\text{-}OOH}$) and the formation rate of PO (r, /s·site) involved in epoxidation reaction *via* "one-step" and "two-step" reaction mechanism at the (a) tetrahedral Ti, (b) Ti/defect and (c) bipodal Ti sites.

Items	(a)	(b)	(c)
"two-step" mechanism			
$\theta_{Ti\text{-}OOH}$	3.40×10^{-17}	4.00×10^{-2}	3.39×10^{-8}
r_2	3.68×10^{-23}	2.85×10^{-2}	6.23×10^{3}
"one-step" mechanism			
$\theta_{H_2O_2}$	4.56×10^{-4}	3.84×10^{-2}	2.48×10^{-2}
$\theta_{C_3H_6}$	5.22×10^{-1}	9.21×10^{-4}	1.04×10^{-1}
r_3	7.42×10^{-12}	7.22×10^{-10}	4.20×10^{-3}

Table S7 The corresponding activation free energy (G_a, kJ/mol), reaction free energies ($\triangle G$, kJ/mol) and the only one imaginary frequency of transition state (v, cm^{-1}) involved in the propylene epoxidation reaction at the nitrided (a) tetrahedral Ti, (b) Ti/defect, (c) bipodal Ti and (d) double embedded bipodal Ti sites, T=313 K and those in parenthesis at 0 K.

Nitrided TS-1 modes	Transition states	G_a, kJ/mol	$\triangle G$, kJ/mol	v, cm^{-1}
Tetrhedral Ti site	TS1-1	75.55(70.10)	-1.55(-8.47)	-183.70
	TS1-2	83.12(83.05)	-179.37(-183.26)	-212.92
	TS1-3	91.52(97.06)	-187.03(-181.93)	-486.34
Ti/defect site	TS2-1	99.92(99.37)	-99.64(-108.29)	-253.75
	TS2-2	47.81(55.44)	-227.49(-223.15)	-385.62
	TS2-1′	44.83(35.80)	-77.17(-86.36)	-389.30
	TS2-2′	48.06(51.62)	-228.99(-229.55)	-406.97
	TS2-3	107.81(104.86)	-287.15(-313.80)	-425.78

Bipodal Ti site	TS3-1	21.70(24.15)	-56.50(-55.83)	-711.34
	TS3-2	58.46(47.69)	-195.37(-207.64)	-419.24
	TS3-1′	23.84(23.18)	-67.24(-68.48)	-742.49
	TS3-2′	62.57(65.42)	-184.29(-192.15)	-516.07
	TS3-3	72.67(68.22)	-237.66(-248.08)	-526.86
Double embedded bipodal Ti site	TS4-1	27.53(25.48)	-83.86(-85.12)	-700.38
	TS4-2	68.68(66.44)	-190.05(-191.86)	-320.23
	TS4-3	71.57(68.09)	-239.33(-246.59)	-442.10

Table S8 The corresponding activation free energy (G_a, kJ/mol), reaction free energies ($\triangle G$, kJ/mol) and the only one imaginary frequency of transition state (v, cm^{-1}) involved in the dissociation of H_2O at the nitrided tetrahedral Ti, Ti/defect, bipodal Ti and double embedded bipodal Ti sites, T=313 K and those in parenthesis at 0 K.

Nitrided TS-1 modes	Transition states	G_a, kJ/mol	$\triangle G$, kJ/mol	v, cm^{-1}
Tetrhedral Ti site	TS1-4	88.90(77.39)	48.09(37.34)	-1091.35
Ti/defect site	TS2-4	52.89(48.14)	-95.75(-105.06)	-336.30
Bipodal Ti site	TS3-4	37.73(34.14)	-58.64(-61.08)	-838.35
Double embedded bipodal Ti site	TS4-4	43.67(37.00)	-68.87(-73.93)	-1015.35

Table S9 The corresponding activation free energy (G_a, kJ/mol), reaction free energies ($\triangle G$, kJ/mol) and the only one imaginary frequency of transition state (v, cm^{-1}) involved in the ring-opening of PO with Ti-OH, Ti-η^1-OOH and Ti-η^2-OOH nucleophiles at the nitrided (a) tetrahedral Ti, (b) Ti/defect, (c) bipodal Ti and (d) double embedded bipodal Ti sites, T=313 K and those in parenthesis at 0 K.

Nitrided TS-1 modes	Transition states	G_a, kJ/mol	$\triangle G$, kJ/mol	v, cm^{-1}
Tetrhedral Ti site	TS1-5	266.29(252.77)	-8.95(-23.83)	-647.04
	TS1-5′	206.22(197.23)	-40.79(-54.72)	-568.29
	TS1-6	175.15(164.31)	-23.74(-33.61)	-491.23
	TS1-6′	228.33(215.70)	-67.11(-80.47)	-632.65
	TS1-7	153.07(139.02)	-63.36(-74.32)	-647.91
	TS1-7′	135.23(128.79)	-65.20(-75.46)	-591.15
	TS1s	185.39(185.96)	-11.53(-19.00)	-725.86
	TS1s′	213.76(208.08)	-44.13(-52.58)	-552.57
Ti/defect site	TS2-5	179.06(174.64)	-69.29(-77.63)	-592.21
	TS2-5′	200.20(193.50)	-85.03(-90.99)	-616.89
	TS2-6	143.35(142.84)	-65.96(-69.60)	-518.43
	TS2-6′	174.37(172.28)	-78.99(-87.02)	-585.88
	TS2-7	96.79(93.75)	-66.55(-72.88)	-244.24

	TS2-7′	104.93(108.70)	-83.22(-90.81)	-315.15
	TS2-8	98.91(93.68)	-69.27(-76.65)	-319.63
	TS2-8′	120.38(118.88)	-86.97(-92.59)	-362.74
	TS2s	233.75(233.52)	-38.27(-51.04)	-571.61
	TS2s′	204.76(199.48)	-51.36(-63.90)	-522.42
Bipodal Ti site	TS3-5	157.07(172.01)	-50.79(-51.04)	-524.28
	TS3-5′	177.82(188.66)	-67.63(-69.05)	-592.63
	TS3-6	128.84(142.47)	-44.17(-49.27)	-454.99
	TS3-6′	174.31(179.32)	-72.69(-68.11)	-553.11
	TS3-7	154.70(160.52)	-75.30(-70.13)	-421.99
	TS3-7′	104.42(110.44)	-70.55(-67.55)	-347.93
	TS3-8	116.15(118.18)	-105.87(-108.31)	-365.53
	TS3-8′	111.60(99.90)	-69.64(-70.74)	-375.48
	TS3-9	93.71(96.24)	-67.09(-65.62)	-303.48
	TS3-9′	111.58(117.85)	-82.32(-82.44)	-382.15
Double embedded	TS4-5	133.18(135.59)	-96.36(-100.42)	-362.05
bipodal Ti site	TS4-5′	166.13(169.76)	-95.25(-96.86)	-433.83
	TS4-6	132.24(133.28)	-73.70(-72.74)	-346.76
	TS4-6′	161.29(156.15)	-105.33(-110.28)	-436.76
	TS4-7	136.81(140.18)	-89.47(-86.85)	-405.20
	TS4-7′	115.42(116.21)	-99.37(-104.24)	-333.04
	TS4-8	92.14(91.64)	-80.19(-76.83)	-313.52
	TS4-8′	100.94(103.40)	-93.28(-94.88)	-312.14

Table S10 The adsorption free energy of H_2O or CH_3OH (G_{ads}, kJ/mol), the activation free energy (G_a, kJ/mol), reaction free energy (ΔG, kJ/mol) and the only one imaginary frequency of transition state (v, cm^{-1}) involved in PG, SPM and PPM formation *via* "two-step" reaction mechanism at the nitrided tetrahedral Ti, Ti/defect, bipodal Ti and double embedded bipodal Ti sites at 313 K.

Nitrided TS-1 modes	Transition states	G_{ads} (kJ/mol)	G_a (kJ/mol)	ΔG (kJ/mol)	v (cm^{-1})
Tetrhedral Ti site	TS1-8	-40.93(-29.70)	198.34(188.81)	33.72(30.38)	-367.19
	TS1-8′	-34.11(-25.03)	235.35(233.84)	29.10(30.43)	-400.77
	TS1-9	-35.12(-21.12)	196.98(204.52)	38.09(33.72)	-419.45
	TS1-9′	-29.32(-13.35)	174.12(172.84)	5.88(1.88)	-323.24
Ti/defect site	TS2-9	-18.89(-7.01)	62.37(51.77)	-7.20(-12.11)	-236.08
	TS2-9′	-8.73(7.58)	195.44(180.99)	-14.66(-26.25)	-365.96
	TS2-10	-19.00(-1.49)	25.08(26.06)	-38.17(-37.58)	-249.14
	TS2-10′	-8.08(9.74)	114.99(119.43)	-25.58(-26.67)	-318.24
Bipodal Ti site	TS3-11	-65.56(-59.52)	80.24(85.14)	-64.02(-62.65)	-296.27
	TS3-11′	-28.46(-13.87)	141.96(138.95)	-4.19(-11.18)	-356.34
	TS3-12	-20.62(-5.29)	75.68(64.82)	-15.71(-23.69)	-340.92

	TS3-12′	-9.86(-2.14)	180.99(182.42)	-56.70(-48.76)	-371.20
Double embedded	TS4-9	-29.68((-23.51)	123.88(130.80)	-18.58(-20.96)	-310.08
bipodal Ti site	TS4-9′	-46.50(-40.28)	233.10(229.19)	42.31(38.27)	-398.46
	TS4-10	-1.52(5.21)	195.94(209.89)	-33.06(-34.11)	-403.01
	TS4-10′	-40.93(-26.92)	183.32(178.83)	24.60(14.71)	-382.86

S9 Definitions of desorption barrier and PO selectivity

Once the target product is formed at the catalytically active Ti site, there will be two paths: (1) desorption from the active site *via* overcome one desorption energy barrier; (2) ring-opening and conversion into by-products at the active site through an activation energy barrier. Previous studies have shown that the desorption barrier is approximately equal to the absolute value of adsorption energy,[16] therefore, the adsorption energy of PO is used as its' desorption barrier. Therefore, the selectivity of propylene epoxidation to PO is evaluated by the difference between the overall barrier of side reaction and it desorption barrier, which is denoted according to the formula: $\triangle G_a = G_a - |G_{ads}|$, where G_a is the overall energy barrier of PO conversion into by-products, and G_{ads} is the corresponding adsorption free energy of PO.[17] With above definition, the higher value of $\triangle G_a$, the better selectivity of PO.

S10 Comparison of Brønsted/Lewis acidity

The Ti in active site is considered the Lewis acid because it can accept electrons, therefore, the strengths of Lewis acid can be investigated through exploring the geometry parameters, Mulliken charge, vibrational frequency and adsorption energy of the probe CO molecule absorbed on Ti active sites.[18] The CO molecule bears a positive charge when it is adsorbed on active sites, simultaneously the charge on Ti is became smaller with the formation of the adsorbed complex, electrons transfer from the CO molecule to the Ti when CO adsorbed on active sites.

The strength of Brønsted acidic protons in nucleophile can be investigated through using trimethylphosphine oxide (TMPO) as the probe molecule.[19] The most obvious change after the adsorption of TMPO on different Brønsted protons of nucleophiles are the formation of hydrogen bond between TMPO and Brønsted acidic protons, and the notable increase of P-O bond length in TMPO compared to that of the bare TMPO. These are indicated that the occurrence of proton transfer from the host (Brønsted acid site) to the guest (TMPO), forming $TMPOH^+$ cationic complex as consequence. The greater the change, the easier the proton transfer to TMPO, the stronger the Brønsted acidity. In addition, TMPO is adsorbed on the acid site, and the acid strength can also be determined by investigating the change of the stretching vibration frequency of O-H on the acid site. The hydrogen bond between TMPO and the H of the acid site will naturally weaken the chemical bond of O-H and shift the stretching vibration

frequency of O-H to the lower frequency. The larger the shift, the stronger the weakening of the O-H bond, the stronger the hydrogen bond formation here, indicating that the acidity is stronger.

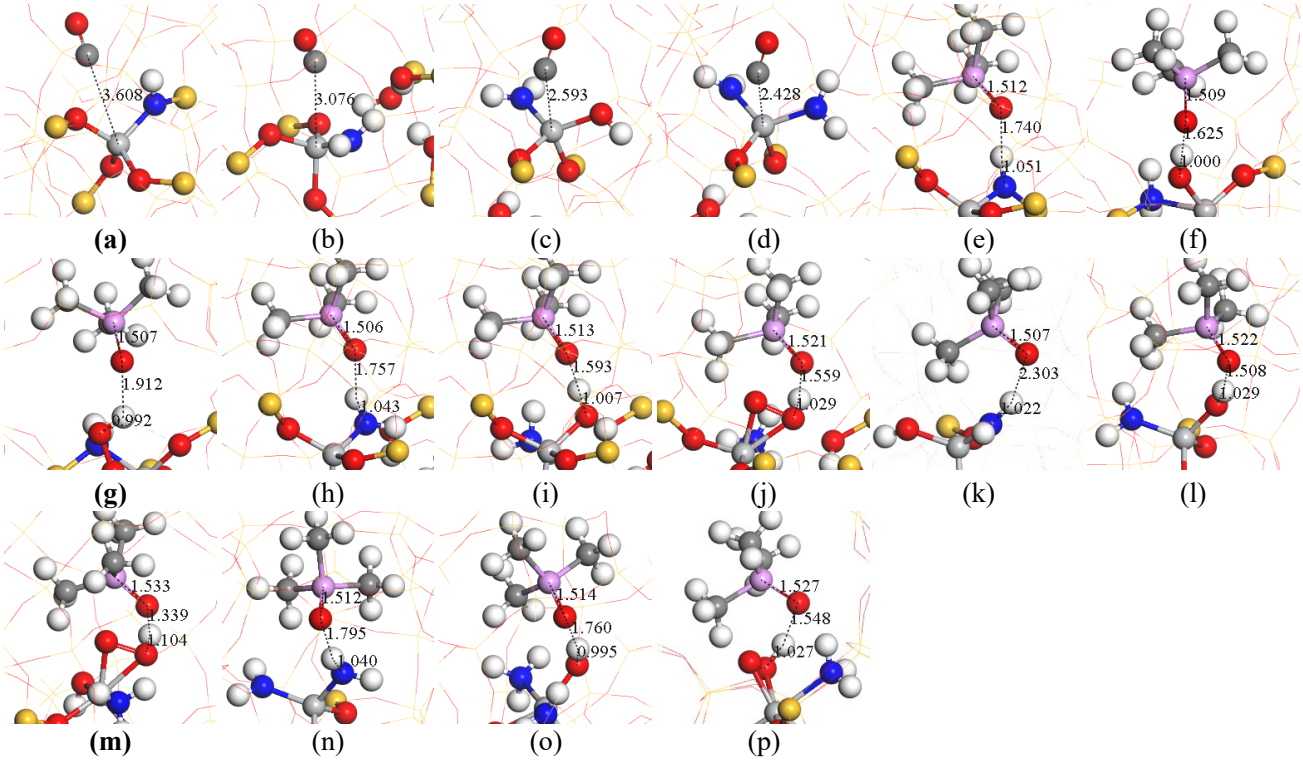

Fig. S20 The Optimized geometries of CO molecule adsorbed on nitrided (a) tetrahedral Ti, (b) Ti/defect, (c) bipodal Ti and (d) double embedded bipodal Ti sites; the optimized geometries of the TMPO molecule adsorbed on different Brønsted protons of nucleophiles (e) Ti-O(H)-Si (nitrided tetrahedral Ti site), (f) Ti-OH (nitrided tetrahedral Ti site), (g) Ti-η^1-OOH (nitrided tetrahedral Ti site), (h) Ti-NH_2 (nitrided Ti/defect site) (i) Ti-OH (nitrided Ti/defect site), (j) Ti-η^2-OOH (Ti/defect site), (k) Ti-NH_2 (bipodal Ti site), (l) Ti-OH (bipodal Ti site), (m) Ti-η^2-OOH (bipodal Ti site), (n) Ti-NH_2 (double embedded bipodal Ti site), (o) Ti-OH (double embedded bipodal Ti site) and (p) Ti-η^2-OOH (double embedded bipodal Ti site). The bond length is in Å (Ti = light grey, C = grey, O = red, Si = yellow, H = white).

Table S11 Mulliken charges (|*e*|) of C_{CO}, O_{CO} and Ti atoms, adsorption energy (E_{ad}, kJ/mol) and vibrational frequency (v, cm^{-1}) for CO adsorbed on nitrided tetrahedral Ti, Ti/defect and bipodal Ti sites.

Parameters	Mulliken charges (|*e*|)			Adsorption energy	Vibrational frequency
	C_{CO}	O_{CO}	Ti	(CO, kJ/mol)	(CO, cm^{-1})
CO molecule	0.096	-0.096	--	--	2114.57
Nitrided tetrahedral Ti site	--	--	1.011	--	--
CO…Nitrided tetrahedral Ti site	0.122	-0.115	1.007	-10.13	2114.23
Nitrided Ti/defect site	--	--	0.982	--	--
CO…Nitrided Ti/defect site	0.138	-0.112	0.946	-13.97	2113.97
Nitrided bipodal Ti site	--	--	1.052	--	--
CO…Nitrided bipodal Ti site	0.201	-0.093	0.915	-15.05	2125.90
Double embedded bipodal Ti site	--	--	0.928	--	--
CO…Bipodal Ti site	0.203	-0.106	0.787	-2.29	2089.93

Table S12 The vibrational frequency of hydroxyl (v_{OH}, cm^{-1}) on different Brønsted protons of nucleophile; the different of vibrational frequency of hydroxyl before and after TMPO adsorption on different Brønsted protons (Δv_{OH}, cm^{-1}) of nitrided TS-1 catalyst.

Brønsted protons	v_{OH}	Δv_{OH}
Ti-N(H)-Si (nitrided tetrahedral Ti site)	3505.01	506.32
Ti-OH (nitrided tetrahedral Ti site)	3776.97	671.69
Ti-η^1-OOH (nitrided tetrahedral Ti site)	3493.87	71.83
Ti-NH_2 (nitrided Ti/defect site)	3461.44	324.81
Ti-OH (nitrided Ti/defect Ti site)	3591.63	534.94
Ti-η^2-OOH (nitrided Ti/defect Ti site)	3320.29	565.68
Ti-NH_2 (nitrided bipodal Ti site)	3758.33	440.18
Ti-OH (nitrided bipodal Ti site)	3723.74	495.57
Ti-η^2-OOH (nitrided bipodal Ti site)	3578.00	765.62
Ti-NH_2 (double embedded bipodal Ti site)	3531.43	408.92
Ti-OH (double embedded bipodal Ti site)	3754.57	508.58
Ti-η^2-OOH (double embedded bipodal Ti site)	3440.95	706.53

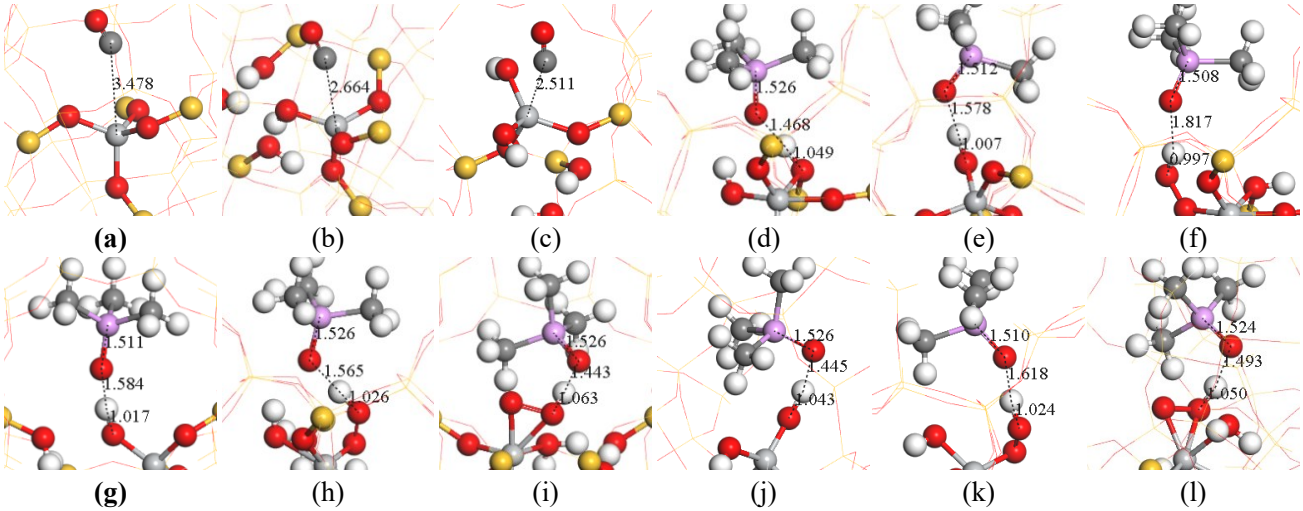

Fig. S21 The Optimized geometries of CO molecule adsorbed on (a) tetrahedral Ti site, (b) Ti/defect and (c) bipodal Ti site; the optimized geometries of the TMPO molecule adsorbed on different Brønsted protons of nucleophiles (d) Ti-O(H)-Si (tetrahedral Ti site), (e) Ti-OH (tetrahedral Ti site), (f) Ti-η^1-OOH (tetrahedral Ti site), (g) Ti-OH (Ti/defect site), (h) Ti-η^1-OOH (Ti/defect site), (i) Ti-η^2-OOH (Ti/defect site), (j) Ti-OH (bipodal Ti site), (h) Ti-η^1-OOH (bipodal Ti site), (i) Ti-η^2-OOH (bipodal Ti site). The bond length is in Å (Ti = light grey, C = grey, O = red, Si = yellow, H = white).

Table S13 Mulliken charges (|*e*|) of C_{CO}, O_{CO} and Ti atoms, adsorption energy (E_{ad}, kJ/mol) and vibrational frequency (v, cm^{-1}) for CO adsorbed at the tetrahedral Ti, Ti/defect and bipodal Ti sites.

Parameters	Mulliken charges (|*e*|)			Adsorption energy	Vibrational frequency
	C_{CO}	O_{CO}	Ti	(CO, kJ/mol)	(CO, cm^{-1})
CO molecule	0.096	-0.096	--	--	2114.57
Tetrahedral Ti site	--	--	1.152	--	--
CO…Tetrahedral Ti site	0.132	-0.113	1.143	-33.19	2107.38
Ti/defect site	--	--	1.146	--	--
CO…Ti/defect site	0.207	-0.096	1.053	-23.19	2164.77
Bipodal Ti site	--	--	1.193	--	--
CO…Bipodal Ti site	0.237	-0.079	1.020	-26.06	2156.44

Table S14 The vibrational frequency of hydroxyl (v_{OH}, cm^{-1}) on different Brønsted protons of nucleophile; the different of vibrational frequency of hydroxyl before and after TMPO adsorption on different Brønsted protons (Δv_{OH}, cm^{-1}).

Brønsted protons	v_{OH}	Δv_{OH}
Ti-O(H)-Si (tetrahedral Ti site)	3123.08	736.77
Ti-OH (tetrahedral Ti site)	3754.48	757.69
Ti-η^1-OOH (tetrahedral Ti site)	3544.63	238.61
Ti-OH (Ti/defect site)	2892.22	--
Ti-η^1-OOH (Ti/defect Ti site)	3624.64	841.71
Ti-η^2-OOH (Ti/defect Ti site)	3322.55	1100.12
Ti-OH (bipodal Ti site)	3750.09	1356.80
Ti-η^1-OOH (bipodal Ti site)	3354.78	518.79
Ti-η^2-OOH (bipodal Ti site)	3434.03	616.07

Reference

[1] H. Munakata, Y. Oumi, A. Miyamoto, *J. Phys. Chem. B*, 2001, **105**, 3493-3501.

[2] C. A. Hijar, R. M. Jacubinas, J. Eckert, N. J. Henson, P. J. Hay, K. C. Ott, *J. Phys. Chem. B*, 2006, **104**, 12157-12164.

[3] P. F. Henry, M. T. Weller, C. C. Wilson, *J. Phys. Chem. B*, 2001, **105**, 7452-7458.

[4] G. L. Marra, G. Artioli, A. N. Fitch, M. Milanesio, C. Lamberti, *Micropor. Mesopor. Mat.*, 2000, **40**, 85-94.

[5] C. Lamberti, S. Bordiga, A. Zecchina, G. Artioli, G. Marra, G. Spano, *J. Am. Chem. Soc.*, 2001, **123**, 2204-2212.

[6] J. D. Gale, *Solid State Sci.*, 2006, **8**, 234-240.

[7] B. D. Montejovalencia, J. L. Salcedoperez, M. C. Curetarana, *J. Phys. Chem. C*, 2016, **120**, 2176-2186.

[8] J. C. Dong, H. L. Zhu, Y. J. Xiang, Y. Wang, P. F. An, Y. Gong, Y. X. Liang, L. M. Qiu, A. G. Zheng, X. X. Peng, M. Lin, G. T. Xu, Z. Guo, D. Chen, *J. Phys. Chem. C*, 2016, **120**, 20114-20124.

[9] T. Atoguchi, S. Yao, *J. Mol. Catal. A: Chem.*, 2003, **191**, 281-288.

[10] Q. Qin, Y. Guo, H. Liu, J. Ma, J. Zhu, B. Wang, *Mol. Catal.*, 2023, **543**, 113147.

[11] H. Liu, Q. Qin, J. Zhu, J. Ma, B. Wang, *ACS Appl. Mater. Inter.*, 2022, **14**, 9763-9780.

[12] X. M. Cao, R. Burch, C. Hardacre, P. Hu, *Catal. Today*, 2011, **165**, 71-79.

[13] Y. M. Choi, P. Liu, *J. Am. Chem. Soc.*, 2009, **131**, 13054-13061.

[14] Y. Choi, P. Liu, *J. Am. Chem. Soc.*, 2009, **131**, 13054-13061.

[15] Y. Zuo, M. Liu, T. Zhang , L. Hong, X. Guo, C. Song, Y. Chen, P. Zhu, C. Jayec, D. Fischerc, *RSC Adv.*, 2015, **23**, 17897-17904.

[16] X. M. Cao, R. Burch, C. Hardacre, P. Hu, *Catal. Today*, 2011, **165**, 71-79.

[17] B. Zhao, R. Zhang, Z. Huang, B. Wang, *Appl. Catal. A-Gen.*, 2017, **546**, 111-121.

[18] D. Liu, C. Zhong, *J. Phys. Chem. Lett.*, 2010, **1**, 97-101.

[19] N. Feng, A. Zheng, S. Huang, H. Zhang, N. Yu, C. Yang, S. Liu, F. Deng, *J. Phys. Chem. C*, 2010, **114**, 15464-15472.